BNL-224790-2023-TECH
C-A/AP/700

Simulation of Proton Beams in the AGS Booster with Space Charge

J. Beebe-Wang

August 2023

Collider Accelerator Department
Brookhaven National Laboratory

U.S. Department of Energy
USDOE Office of Science (SC), Nuclear Physics (NP) (SC-26)

DISCLAIMER

Simulation of Proton Beams in the AGS Booster with Space Charge

Joanne Beebe-Wang

August, 2023

Contents

1 Introduction **4**

2 Hybrid Model for Simulations with Space Charge **6**

2.1 Particle in Cell (PIC) Model 6

2.2 Frozen Space Charge Model 7

2.3 Hybrid Space Charge Model 8

3 Required Features and Choice of Booster Simulation Code **9**

4 Physical and Numerical Parameters used in Simulations **11**

4.1 Physical Parameters used in Proton Simulations 11

4.2 Numerical Parameters used in Proton Simulations 12

4.3 Accelerator Model of the AGS Booster 20

5 Injection and Early Stages of the Booster Cycle **21**

5.1 Beam Loss Rates and Locations of Beam Loss 21

5.2 Emittance Growth due to Charge Exchange at the Injection Foil 26

5.3 Effects of Space Charge at Injection Energy 28

5.4 Injection Optimization 33

5.5 Post-injection Optimization 36

6 Full Cycle Simulations **42**

6.1 Events and Timings in a Booster Cycle 42

6.2 Energy Ramping, RF and Tunes during a Booster cycle 43

6.3 Impact of Initial Intensity on a Full Cycle 46

6.4 Impact of Initial Emittance on a Full Cycle 49

6.5 Impact of Initial Momentum Spread on a Full Cycle 53

6.6 Trends in Beam Properties and Parameter Changes 56

7 Summary and discussion **61**

1 Introduction

As higher intensity accelerators are designed, built and operated, the resonances and instabilities caused by space charge can become dominant effects in limiting the intensity of the beam that can be delivered. Particle loss has many causes but space charge can be a major factor in reducing beam intensity and generating emittance growth, particularly at low energies and in the lower energy stages of accelerators such as the AGS Booster. Successful operation relies on a good understanding of basic particle dynamics and it becomes an important challenge to ascertain how the beam evolves when charged particles experience both external forces through the fields of the magnets combined with internal forces through Coulomb interactions.

A possible approach to such a study is to include calculations of space charge in computer simulation codes that track the motions of charged particles in 6D phase space [1]. Unfortunately, repeated space charge calculations in 6D phase space are computationally intensive even with the most modern computing facilities. Study with traditional models of space charge is then either limited to a short real-time scale, or sacrifices accuracy and often omits some of the physics.

The study described in this report attempts to explore all aspects of the Booster from injection, through RF capture and acceleration to the extraction energy. The simulations are allied to real machine settings. They do not attempt to model effects that are well known and for which accurate experimental data are available, but they try in many cases to extend beyond the normal Booster parameter range so as to understand the limitations on operations and suggest areas for improvement.

The initial sections of the Report cover simulation codes in general, explaining the complexities of space charge modeling and the issues in applying them to model Booster operation. The need to perform simulations covering $\sim$10 msec (or many thousand revolutions of the ring) forces one to look for a code containing an adaptable space charge model that can at one extreme deal with a beam that changes very rapidly over a short time scale and at the other extreme handle a beam in which there is only progressive variation over a much longer period. Section 2 describes two models traditionally used

for space charge calculation and introduces an alternative, the hybrid model, that turns out to be applicable to the studies presented in this report.

In Section 3, we list the features of a code necessary to realistically simulate beams in the AGS Booster. Justification is given for choosing "Simpsons" as the simulation code for this study.

In the work that follows, all physical parameters that are functions of time are taken either from operational settings or from run-time read-backs. The numerical parameters are determined through comparison and examination of the results of a large number of test simulations. Their impact on the simulation results and the required CPU times are reported in Section 4.

The simulation studies are performed for the full cycle of injection, RF capture and energy ramping in the Booster. However, it is worth remarking that control and understanding of beam loss are crucial aspects of operating any high intensity circular machine. In general, the causes of beam loss are many and include the following: foil scattering; H^- ions missing the foil; imperfect charge exchange; unoptimized injection parameters; longitudinal beam halo, perhaps related to imperfect beam chopping leading to un-captured beam; unoptimized RF program that allows beam to leak out of the bucket into unstable regions of phase space; transition crossing; extraction issues. Some of these are not the issues on the Booster, and they may be attributed to the basic machine design, and study of others, such as detailed foil scattering and foil breakdown through heating, may be beyond the scope of simulation codes, depending on their sophistication.

The focus in this Report is on issues directly related to space-charge, mainly as a result of emittance increase in the transverse and/or longitudinal planes. Optimization and consideration of possible mitigation strategies are presented sequentially as simulation results for each stage of the complete ring cycle are described.

More detailed study that distinguishes between effects of linear and non-linear space charge, that identifies image charge effects from direct Coulomb interactions, that pushes parameters to the onset of higher order resonances, that explores impedance effects and beam halo formation are all left to a future date.

2 Hybrid Model for Simulations with Space Charge

We look first into the challenges in simulating the beam dynamics in the Booster, with special attention to space charge effects. There are two basic models for space charge simulation: the tried and tested PIC (Particle-In-Cell) method and the more recently developed Frozen Space Charge model. They each have merits in the areas for which they were specifically developed but also show drawbacks when applied to aspects for which they were never intended to be used. In this section, after presenting the two traditional models and their pros and cons, we introduce a third alternative – the hybrid space charge model – which is aimed at some kind of reconciliation and has accordingly been adopted for this simulation study.

2.1 Particle in Cell (PIC) Model

The idea of evaluating the space charge potential using macro-particles came from plasma physics. A simplistic way of calculating the space charge potential is to sum the binary interactions between all macro-particles in the ensemble (Particle-Particle or PP method). It is not efficient from the computational point, though has been used to study beam dynamics in individual modules such as an RFQ, and suffers from a graininess caused by the limited number of macro-particles that, to some extent, can be smoothed out by more advanced mathematical techniques. A more practical approach is to divide the configuration space using a grid and then allocate macro-particles to and calculate the Coulomb potential at each grid point. This is called the Particle in Cell (PIC) model.

In a PIC model, all the real particles in the beam are represented by a given number of macro-particles. Each macro-particle carries the total weight and charge of the cluster of real particles it represents. The total time period during which the beam is tracked is also divided into a number of time-steps. Within each time step, the model calculates the motion of each macro-particle based on the electromagnetic field of the macro-particle's location

along the accelerator, as well as the space charge force from the other macro-particles that was calculated from the previous time step. At the end of each time step, the 6D-coordinates of all macro-particles are recorded, and space change forces are recalculated based on the relative locations of all the macro-particles. This newly calculated set of space charge forces, together with the electromagnetic fields at each of the macro-particle's new locations, are applied to the macro-particles during the next time step.

The total number of macro-particles is generally much less (by several orders of magnitude) than the number of real particles, and this may introduce non-physical effects. One example is the "numerical intrabeam scattering", which causes continuous emittance blowup [2].

Some of the existing tracking codes including the PIC model for space charge simulation have been used at BNL. A brief description of the methods used in each code and a comparison of their results were reported in Reference [3].

2.2 Frozen Space Charge Model

In a (so-called) frozen space charge model, the space charge potential is calculated from the initial distribution of particles. Space charge forces from this potential are applied to the beam as if the particle distribution does not change, or changes only very slowly, during the tracking (i.e. the beam is "frozen"). The particle distribution and space charge potential are updated according to the rate of evolution while tracking, but the time period between updates can correspond to one or more revolutions of the ring and be much longer than a single time step.

This method is not a self-consistent calculation. However, for cases where the space charge effects are regarded as small perturbations, the change of the charge distribution, and therefore the change of the space charge potential, is negligible and the beam behavior is mainly determined by the external lattice elements.

In fact, space charge effects in rings are relatively small because the periodic structure excites resonances and tune shift can be sufficiently small that

the approximation is well justified. The advantage is that it is free from the numerical noise which the PIC method cannot avoid and can make the whole tracking exactly symplectic. On the other hand, instabilities, such as envelope instabilities due to space charge, cannot be modeled [4].

2.3 Hybrid Space Charge Model

The advantage of the PIC model is its higher accuracy since it tracks all the macro-particles and calculates the space charge potential from all the macro-particles on each step. Its disadvantage is the need for a large number of macro-particles (several millions). This makes the PIC model slow and not suitable for long-term tracking. The advantage of the frozen space charge model is its speed. Its disadvantage is its lower accuracy, especially when the charge distribution changes rapidly, such as during RF capture, without an update to the potential.

In recent years activities in higher intensity accelerator designs have placed increasing demand on long term space charge tracking, and this has resulted in a "hybrid model" being developed, implemented, tested and benchmarked with run-time measurements.

One of the tracking codes capable of using the hybrid model to simulate space charge effects is Simpsons [5]. Simpsons is widely recognised for its use in the design of the J-PARC synchrotrons and for the success of its use when allied to experiment in upgrading the spallation neutron source to operate above the 1 MW level.

The two key points of the hybrid model implemented in Simpsons are:

1. In the longitudinal direction, the code tracks a reasonable number of macro-particles (5k to 20k) to reconstruct the longitudinal beam profile by
    - binning the beam into ∼50 longitudinal slices;
    - decomposing each slice using Fourier techniques;

- reconstructing the longitudinal profile by using only low order Fourier components in order to cut off the high frequency noise.

2. In the transverse plane, the code calculates the RMS emittance of the entire beam every turn to update the frozen space charge potential. The charge distribution is kept the same, e.g. Gaussian or Waterbag. A space charge kick is then applied to all macro-particles.

In this way the transient behavior of the bunch shape is modeled without the need for a very large number (>1M) of macro-particles, and the simulations can be carried out within a reasonable CPU time.

In common with other macro-particle tracking codes with space charge, beam development in Simpsons is carried out in two parts. The first operation updates macro-particle coordinates as a result of space charge effects integrated in each small time step. The second part advances macro-particle coordinates in the same time period, through application of the external lattice elements. Separation into two parts, which are carried out in alternating fashion, is considered important in order to take into account local details of the beam envelope and the s-dependent space charge potential, where s is the direction of the beam travel. If the beam emittance in transverse and longitudinal directions evolves, the space charge potential is updated so that the calculations are self-consistent. Both parts of Simpsons are symplectic, which is an essential feature in any code suitable for long term tracking, and minimise growth of machine errors and numerical noise [6].

The hybrid model in Simpsons has been benchmarked with run-time measurements at J-PARC 3 GeV RCS with a very good agreement [7, 8].

3 Required Features and Choice of Booster Simulation Code

Turning to the challenges in simulating the beam dynamics in the Booster cycle, the following features need to be studied carefully to understand beam behavior and the causes of beam loss.

1. Multi-turn injection including the effects of the charge exchange foil and the 4D injection bump as a function of time.

2. The transition between the initial coasting beam, through RF capture to a bunched beam state.

3. Energy ramping.

4. Rapid changes in the longitudinal charge distribution (considered as variations in peak line density). Some progress can be made with a purely longitudinal code but accurate modeling may require a fully 6D code.

5. RF voltage changes throughout the cycle with a coasting beam, RF capture and energy ramping. This suggests treating the 1^{st} and 2^{nd} RF voltage profiles and the relative phase as tables with interpolation with short time step.

6. Both horizontal and vertical tunes change considerably during a cycle, and quadrupole currents need to be included in the code as functions of time.

7. Different physical apertures at different elements (Bend, Quad and Sext) are required for accurate beam loss estimates.

Some of above features were already implemented into Simpsons and the remainder have recently been added specifically for the Booster study. [1] It was clear that Simpsons, in comparison with the other space charge codes available, contained all the features deemed necessary for the Booster study.

Simpsons is capable of tracking using any one of the three space charge models PIC, frozen and hybrid model (see §2). For reasons discussed in §2.3, the advantages of the hybrid model made it the choice for this study.

[1] The author expresses grateful thanks to Dr Shinji Machida, the author of the Simpsons code, for the additional features and his advice on their use.

4 Physical and Numerical Parameters used in Simulations

4.1 Physical Parameters used in Proton Simulations

All physical parameters as represented as functions of time taken either from operational settings or from run-time read-backs. Table 1 lists the most important physical parameters of the Booster used in the simulations.

Table 1: Physical parameters used in the simulations of proton beams in the AGS Booster.

Parameter	Injection	$G\gamma = 3$	$G\gamma = 4$	Extraction
$G\gamma$	2.175007	3.0	4.0	4.5
W [MeV]	200.0	631.753	1155.095	1416.766
cp [GeV]	0.644445	1.258819	1.871318	2.160058
E [GeV]	1.138272	1.570026	2.093367	2.355038
$B\rho$ [Tm]	2.149636	4.198969	6.242046	7.205178
β	0.566160	0.801783	0.893927	0.917207
γ	1.213158	1.673316	2.231088	2.509974
η	-0.6362	-0.3143	-0.1581	-0.1159
h	1	1	1	1
hf [MHz]	0.841167	1.191240	1.328143	1.362779
R [m]	$201.78/2\pi$	$201.78/2\pi$	$201.78/2\pi$	128.453/4

Physical apertures are taken to be the inside dimensions of the vacuum chambers. When the transverse excursion of a macro-particle reaches the physical aperture it is considered to be lost from the circulating beam. Particles whose longitudinal excursion goes beyond half the RF bucket length are considered as "potentially lost" since they are then in an unstable region of phase space. But they are retained in the simulation, and their presence has an effect on the space charge, until such time as their enhanced momentum, combined with dispersion, causes them to be physically lost at the machine apertures.

A beam loss parameter is calculated as a function of time and is defined as the fraction of accumulated beam loss to the total beam in the ring when injection completes.

4.2 Numerical Parameters used in Proton Simulations

The total number of particles in the AGS Booster proton beam is of the order of 10^{11}. It is not practical to track all these particles in the simulations even with the most modern computing facilities. Therefore, the total particles in the beam are replaced by a much small number of macro-particles. Each macro-particle represents a certain number of real particles depending on the "weight" assignment. To accurately study the beam evolution during the Booster cycle it is important to represent the real beam with a sufficiently large number of macro-particles, with an initial 6D distribution that is a good approximation to reality. The distribution can be projected into a transverse distribution in 4D phase space and a longitudinal distribution in 2D phase space.

The choice of a suitable number of macro-particles is a balance between maintaining computational accuracy and controlling the CPU running time. The process is carried out for coasting beams (without longitudinal substructure) and bunched beams (where the longitudinal substructure must be taken into account) separately. The number of macro-particles is chosen to be one that can safely represent the real beam while it is either un-bunched or bunched.

Figure 1 compares the transverse emittance of coasting beams during injection simulated with 2000, 6000, 10000 and 20000 macro-particles. A comparison of transverse emittance, longitudinal emittance, bunching factor and beam loss parameter in the corresponding the bunched beam case is shown in Figure 2 and 3.

To determine the minimum acceptable number of macro-particles for the modeling, we need to identify a criterion. We consider a number of macro-particles to be "suitable" if the simulation results produced are within 5% of convergent results produced with increasingly large numbers of macro-particles. It is found that convergence in measurable quantities is reached

with about 20000 macro-particles in the coasting beam case, and 50000 for bunched beams. The comparison suggests that 5000 macro-particles is adequate for all the simulations in this study.

Figure 4 shows the linear relationship between the CPU assumption and the total number of macro-particles. The data-points in the gray shaded area are considered to be "forbidden" owing to inaccuracies in the results the simulations may produce.

Another important numerical parameter is the time step-size during the tracking. Figure 5 compares the horizontal and vertical emittance of the full Booster cycle, during which the beam evolves from being coasting to bunched, with different time step-sizes.

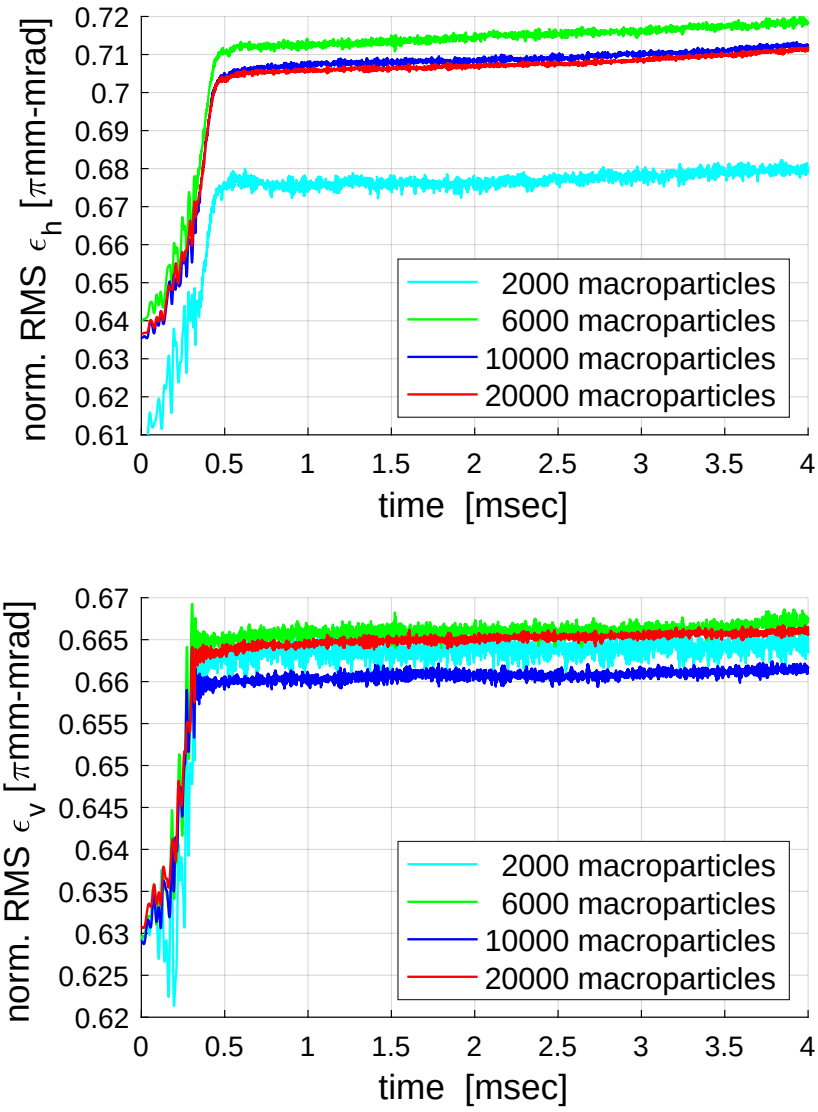

Figure 1: Simulated emittance in the horizontal (ϵ_h) and vertical (ϵ_v) directions vs.time with 2000, 6000, 10000 and 20000 macro-particles. All simulations are with 9×10^{11} protons at set-tunes of $Q_x = 4.5410, Q_y = 4.5555$.

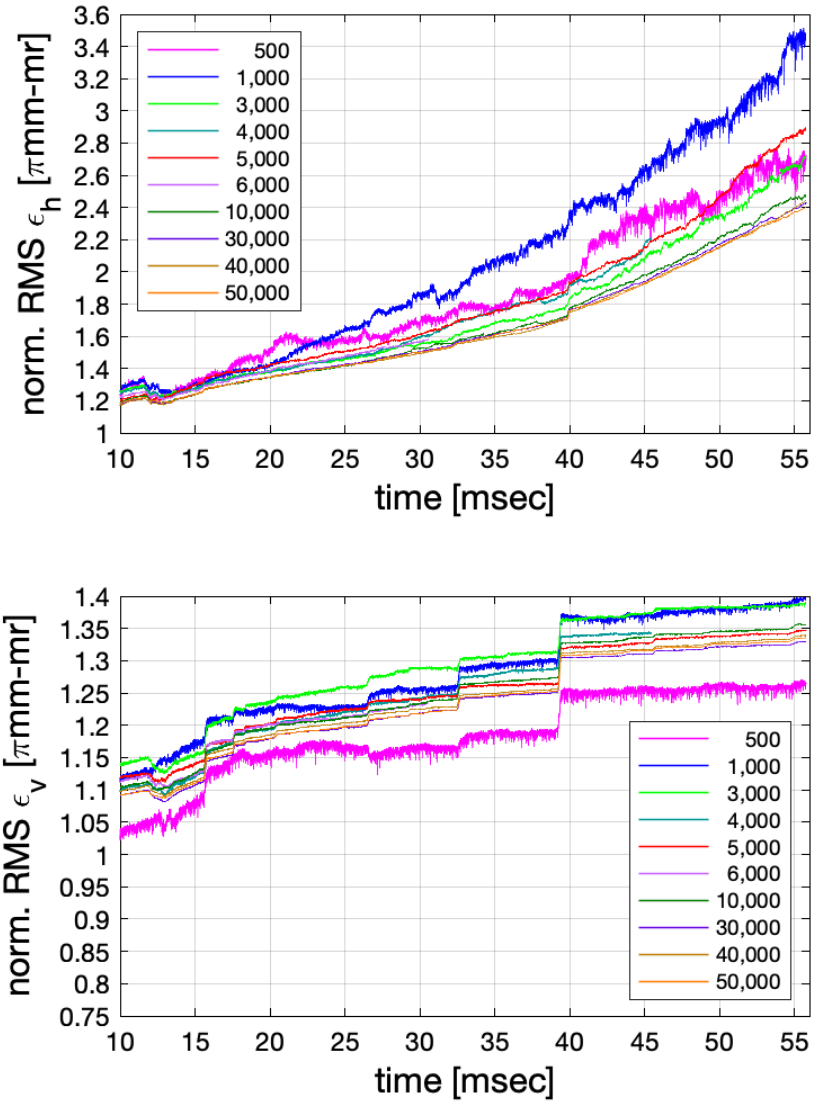

Figure 2: Simulated RMS emittances in the horizontal (ϵ_h) and vertical (ϵ_v) directions against time for different numbers of macro-particles. Simulations were carried out using the Simpsons modeling code.

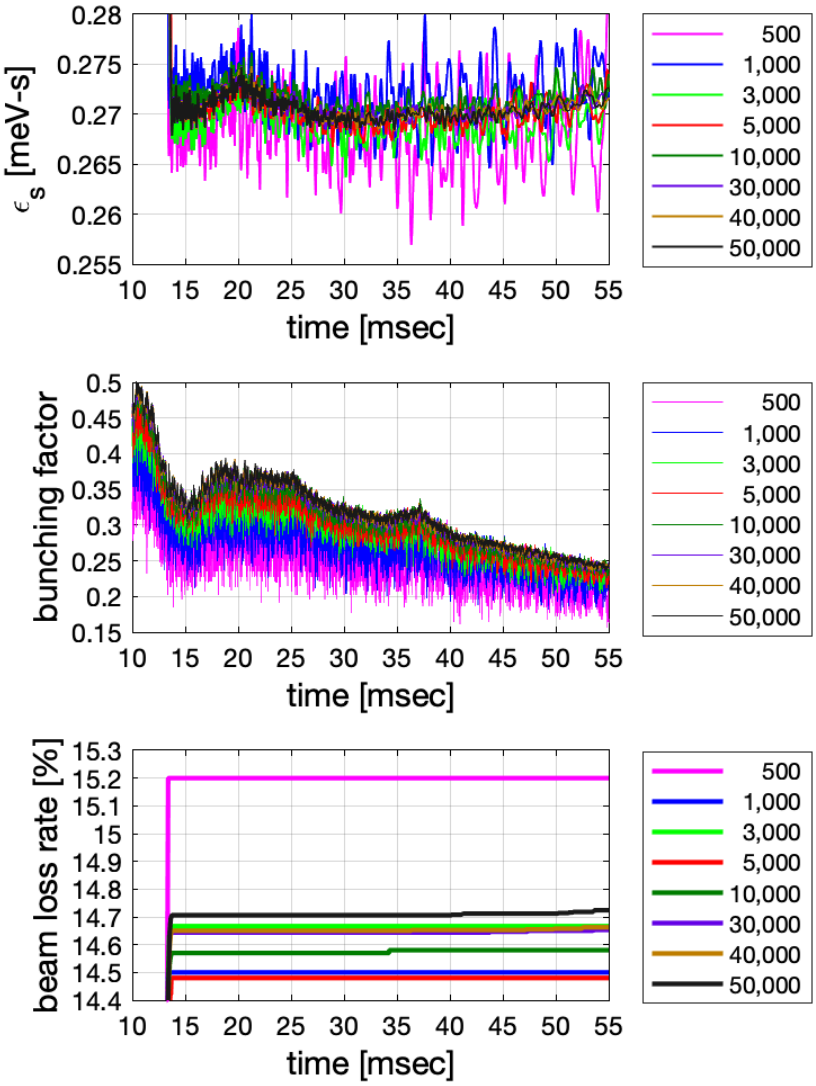

Figure 3: Beam loss parameter and bunching factors against time for different numbers of macro-particles. Simulations carried out using the Simpsons modeling code.

In a similar way, a "suitable" integration step-size can be identified by considering the convergence of results as the time step is made smaller and smaller. A time step is considered "suitable" if the results it produces are within 5% of the convergent results. Convergence is certainly reached with steps greater than 0.1 ns and the analysis suggests that a time step of 10 nsec can be realistically used.

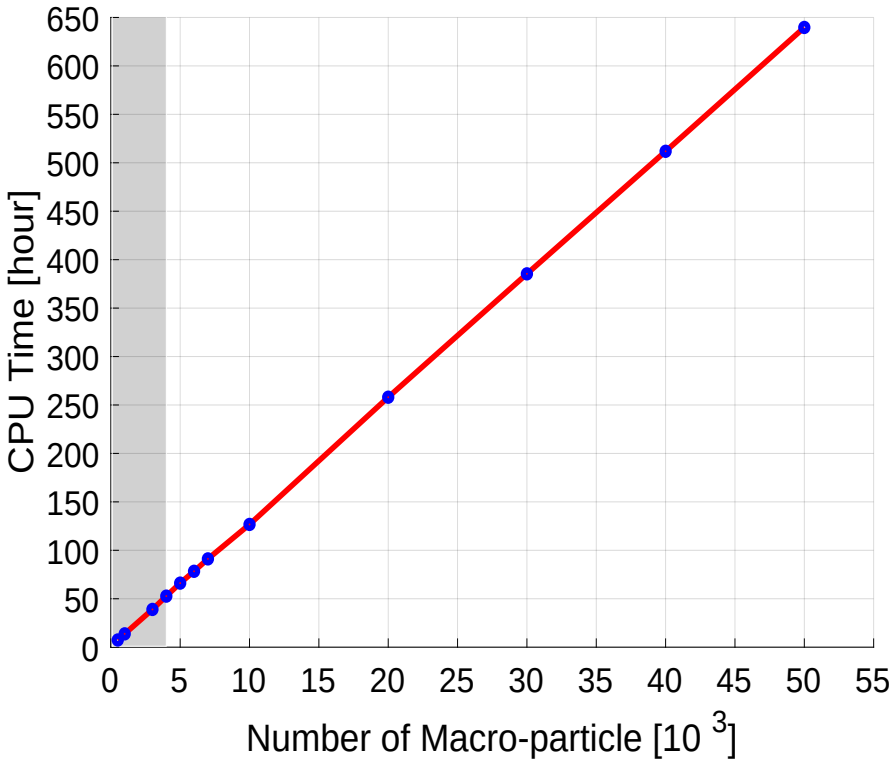

Figure 4: CPU against number of macro-particles.

Figure 6 shows the relationship between the CPU assumption and the time step-size. The data-points in the gray (shaded) area may be suspect due to inaccuracies in results the modeling techniques may produce.

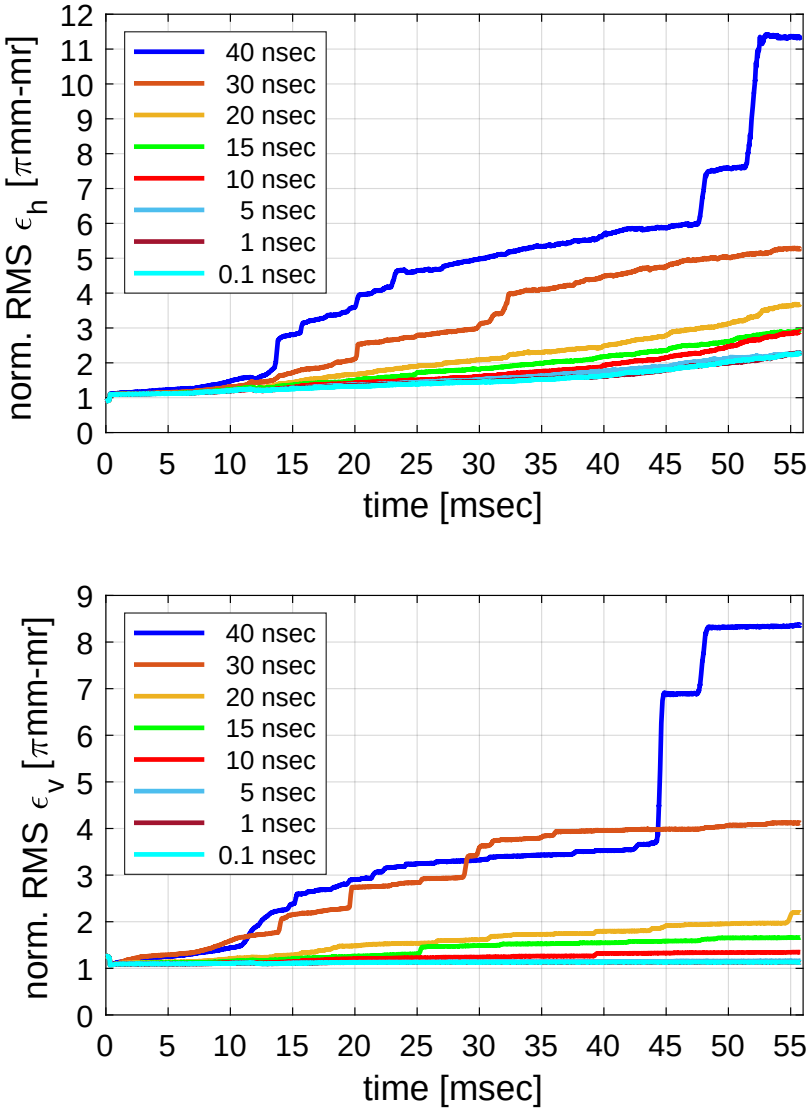

Figure 5: RMS emittances in the horizontal (ϵ_h) and vertical (ϵ_v) directions simulated with different time steps (units: nsec).

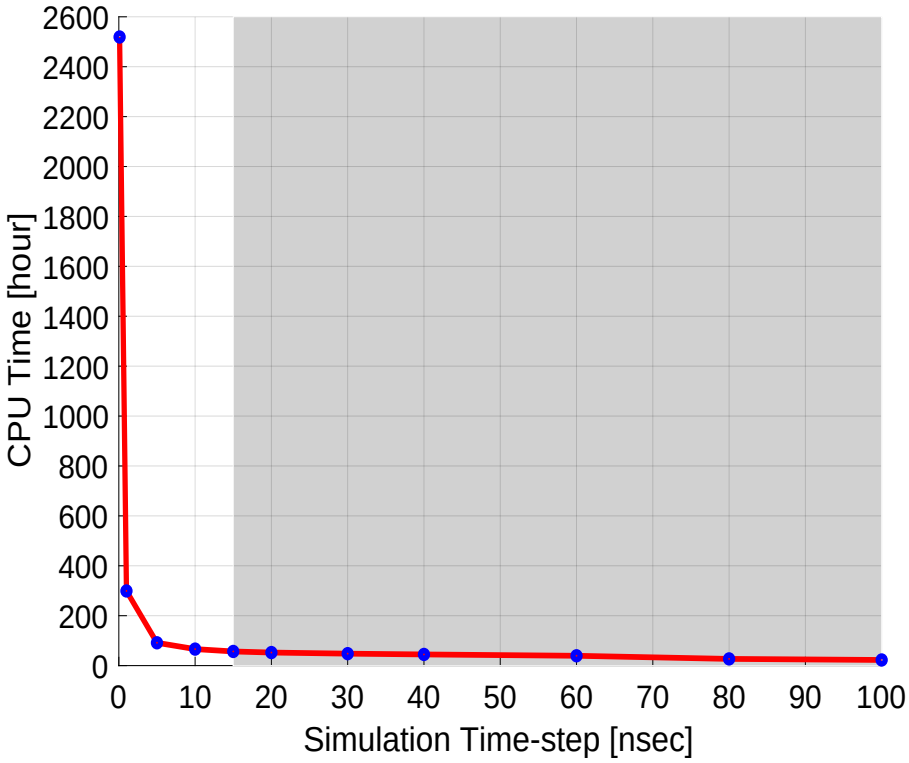

Figure 6: CPU against time step.

4.3 Accelerator Model of the AGS Booster

The magnets, primary RF and higher harmonic RF cavities, beam monitoring elements and other machine elements are based on the standard MADX model of the AGS Booster. The Booster lattice description was converted from MADX format into a TEAPOT input file, and the output from TEAPOT was used as the input for Simpsons simulations, supplying details of machine optics and lattice parameters at all elements around the ring.

Some modifications and adjustments to the standard Booster model are achieved through re-calculating and modifying the strengths and parameters of elements for the whole ring. Each simulation run with Simpsons is carried out in two stages. The first sets up the Booster optical parameters as functions of time (pass1). In the second stage, the ensemble of macro-particles is tracked through the fields of each element of the ring and space charge forces are calculated from the macro-particle distribution (pass2).

In addition to the input parameters there are more than 10 time-dependent parameters details of which are fed in during the simulation runs. Each of these data file specifies how one or more physical parameters change as a function of time during the running-cycle. Examples of changing parameters include the following:

- $B\rho$ during energy ramping (brho.dat);
- Horizontal and vertical set-tunes (agsbqh.dat and agsbqv.dat);
- The primary and higher harmonic RF voltages and relative phases (vrf.dat and vhrf.dat).

5 Injection and Early Stages of the Booster Cycle

5.1 Beam Loss Rates and Locations of Beam Loss

It is a know fact that the proton beam always loses 10-20% of its intensity during the period from "Booster Input" (event name: Bst-Input) to "Booster Early" (event name: Bst-Early) [10].

Figure 7 shows measurements of beam intensity taken over a 12 hr period of Booster operation in April 2022 [9]. The black line represents "Booster

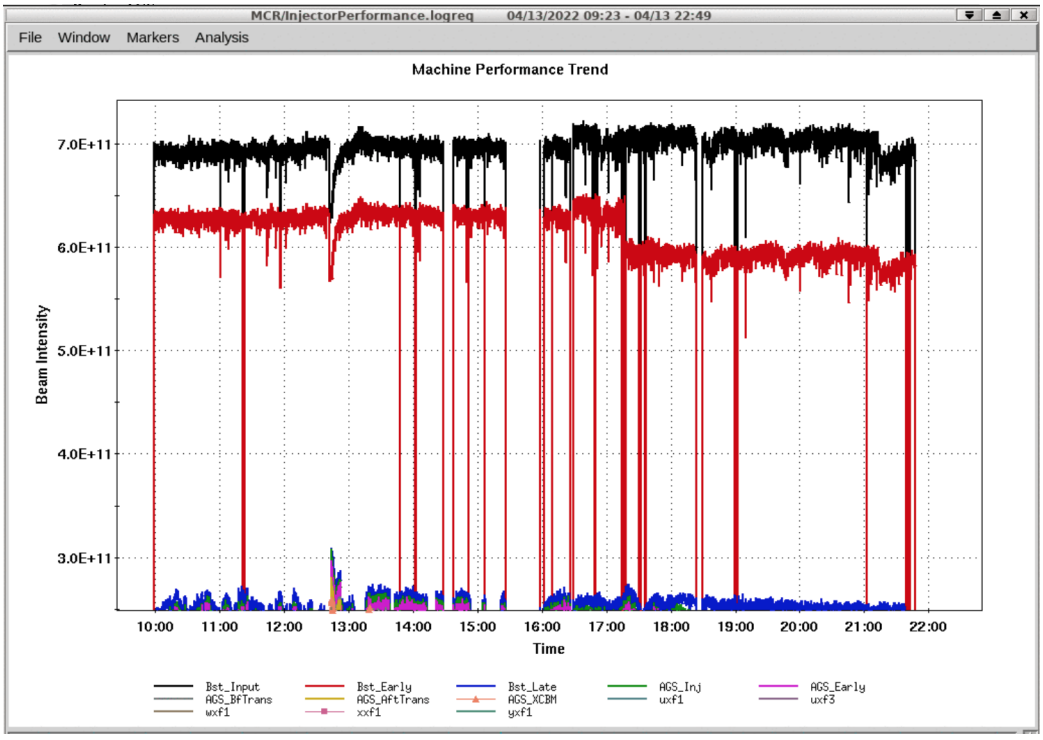

Figure 7: Beam intensity trend during a successful 12 hr period of machine performance, April 13th, 2022. In this latest RHIC proton run (run 2022) both horizontal and vertical scraping was applied.

Input" (event name: Bst_Input), which is the beam intensity measured with a current transformer in the LINAC line, located before the LTB-line. The red line shows "Booster Early" and was obtained from the Booster circulating current measurements at the time marker Bst_Early at Booster time = 73 msec (corresponding to Simpsons time = 1.8 msec). "Booster Late" is represented by the blue line, obtained from the Booster circulating current measurements at the time marker Bst_Late at Booster time = 120 msec (or Simpsons time = 48.8 msec). Finally, the green line is "AGS Injection" (event name: AGS_XCBM), which gives the beam intensity measured with a current transformer in the BTA-line after Booster extraction and before AGS injection. This is regarded as AGS_Inj and is the closest intensity measurement of the Booster extracted beam.

The data was collected during the latest proton run on RHIC (run 2022). During the run, horizontal and vertical scraping was generally applied in the Booster to reduce the transverse emittance in the extracted beam. For this reason, the intensity reduction between "Booster Early" (red line) and "Booster Late" (blue line) in Figure 7 does not represent the natural beam loss in Booster. However, it is evident that beam loss between "Booster Input" (black line) and "Booster Early" (red line) is about 10-15% and appears to have a minimum value of 10%.

Figure 8 shows the beam intensity before, during and after the Booster cycle. Data were collected over a time period of 5 hours during an earlier RHIC proton run on June 28th, 2016 when horizontal and vertical scraping were not applied.

The conclusion can be made, from above two cases and a large number of cases both with and without horizontal and vertical scraping, that a minimum 10% beam loss always exists in the Booster between "Booster Input" (black line) and "Booster Early" (red line).

In order to determine the beam loss rate during this time period, we studied four sets of the intensity measurement data collected over many years of Booster running. Two sets were taken during RHIC operations and two sets were gathered during beam experiments.

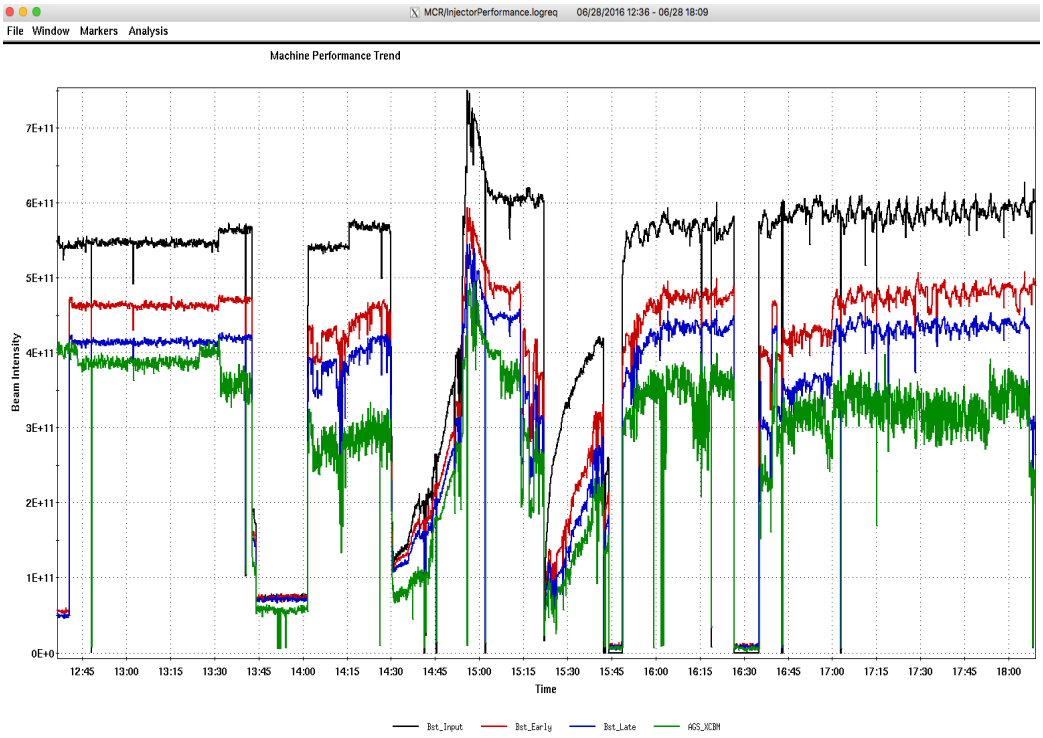

Figure 8: Beam intensity trend before, during and after the Booster cycle during an earlier RHIC proton run when horizontal and vertical scraping were not applied. The color coding is the same as in Figure 7.

All four sets satisfy the following criteria:

1. All the data points in each set were extracted within a few hours of each other;

2. During this period the Booster settings were not changed;

3. With the same Booster settings there was no significant deterioration in the machine operating condition;

4. Over these few hours the Booster was refilled multiple times over a large range of injection intensities. The aim was to acquire data to study beam behavior for varying Booster intensities.

For example, one set of data that satisfies the above criteria has been extracted during the time period shown in Figure 8. The data points are shown as red dots in Figure 9.

Figure 9 shows the beam intensity at "Booster Early" plotted against the intensity at "Booster Input". The four differently colored dots represent the data points of the four different sets. The four colors of the dashed lines are the linear-fits corresponding to data sets of the same color. It can be seen from the figure that all the data sets and their corresponding linear-fits are remarkably close to each other even though they were collected during different days, even in different years. The slopes of the linear-fit range from 0.80 to 0.85 with an average of 0.83, yielding a beam loss rate of 15% to 20% with an average of 17%.

Owing to the similar linear relationship between the beam intensity at "Booster Early" and "Booster Input" we know that the main contribution to the rate of beam loss is intensity independent, even though the beam loss itself is proportional to the total intensity. Also, considering the intensity measurement at "Booster Input" was made before beam injection, we know that the beam loss at the charge exchange foil is included in the total beam loss during the time period from "Booster Input" and "Booster Early".

Now, we estimate the beam loss rate at the location of the injection foil. The LINAC produces an H^- beam from which two electrons are stripped by the foil and injected into the Booster via a non-Liouvillean process. A set of orbit deformation dipoles creates a closed bump at the foil, and varies such that the beam is kept on the foil only during the injection pulse. The LINAC pulse is about 300 μsec long, after which the bump is collapsed and the beam no longer hits the foil.

There is beam loss associated with the stripping efficiency of the charge exchange foil, which depends on the foil material, its thickness and geometry, and the incident energy of the H^- beam. The Booster typically uses a carbon foil of 100 $\mu g/cm^2$ thickness. The incident H^- beam into Booster is typically 200 MeV. Figure 10 shows relative yields of H^-, H^0, and H^+ as a function of foil thickness for a 200 MeV incident H^- beam. From these, the estimated beam loss at the foil is 9%.

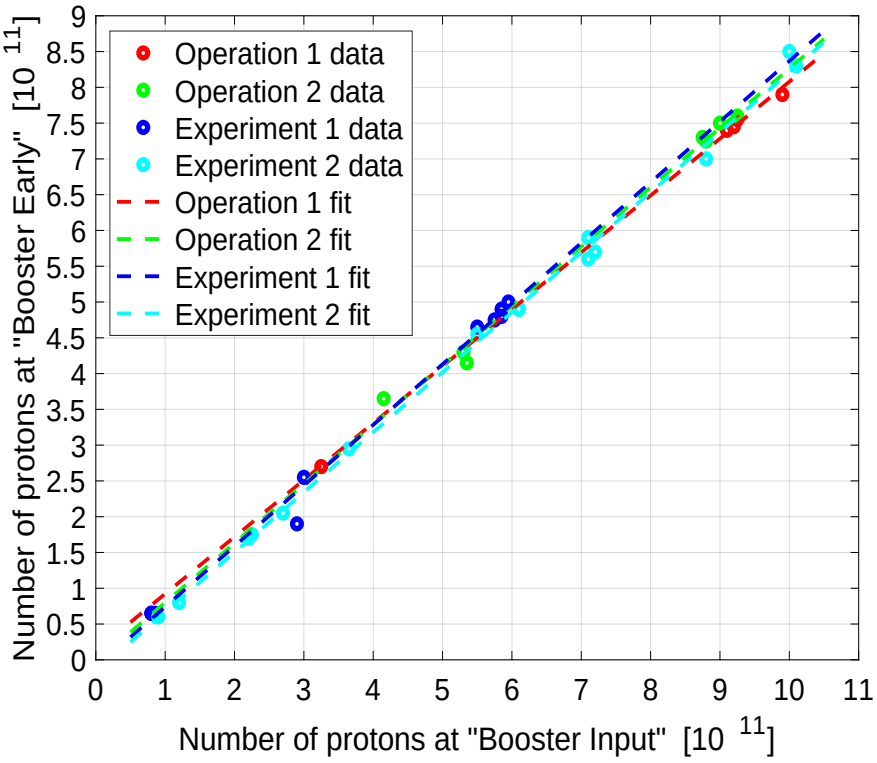

Figure 9: Four sets of the intensity measurement data (two sets from RHIC operations; two sets from beam experiments) collected over multiple Booster runs. Different colors correspond to different sets of data, the dots representing the data points and the dashed lines showing linear fits.

Additionally, there are two other sources of possible beam loss [11]. There is likely loss in the LTB-line up to the order of about 10% and injection mismatch could cause beam loss of an extra few %. Together, these account for a possible injection beam loss of as much as 20%.

From previous work, the beam loss at the foil can be considered to be well understood and realistically estimated. This study focuses on the proton beam that is successfully injected and circulates in the Booster ring, recognizing that this contains 10-20% less than the total number of protons measured at "Booster Input" with a current transformer in the LINAC line.

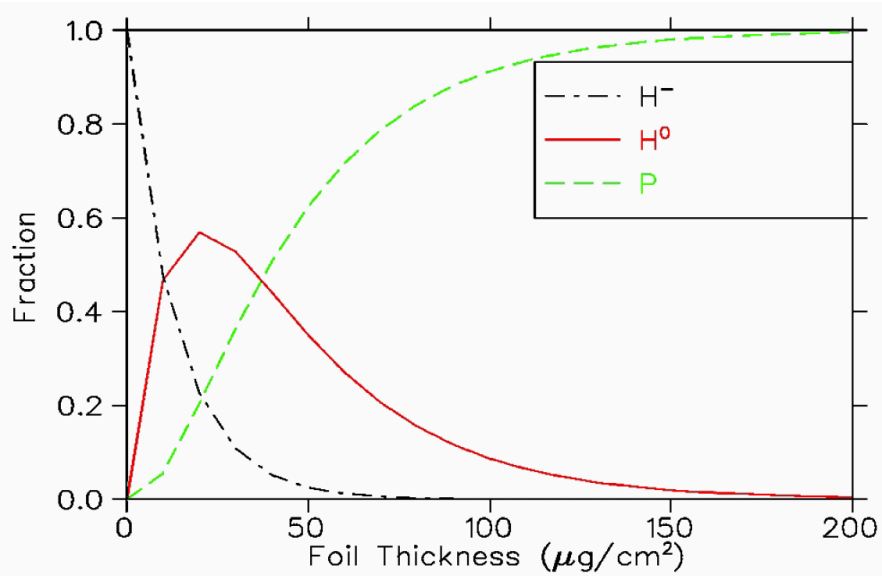

Figure 10: Relative yields of H^-, H^0, and H^+ as a function of carbon foil thickness for a 200 MeV, H^- incident beam.

5.2 Emittance Growth due to Charge Exchange at the Injection Foil

In addition to beam loss, there is emittance growth in the injected beam associated with the charge exchange foil. This emittance growth is mainly caused by multiple scattering of the particles in the foil.

The RMS emittance growth $\Delta\epsilon_{\rm RMS}$ due to multiple scattering can be approximated by [12]

$$\Delta\epsilon_{\rm RMS} = \frac{1}{2} n_{\rm trav}\, \beta_{\rm foil}\, \theta_{\rm RMS} \tag{1}$$

$n_{\rm trav}$ is the number of particle traversals through the foil. All the ions from the linac should pass through the foil and some of the circulating protons may also traverse the foil depending on their position given by the closed orbit bump and their betatron oscillations in the ring. $\beta_{\rm foil}$ is the matched β-function at the foil, and $\theta_{\rm RMS}$ is the RMS multiple scattering per turn,

which depends on the foil material and thickness. In summary, the factors related to emittance growth are foil material, foil thickness, foil geometry, LINAC pulse length and the lattice optics at the foil.

The degree of emittance growth attributable to the foil can be simulated in the Simpsons code using the function (1) and tracking the contribution of each macro-particle as it passes the location of the foil. However, an experimental study was carried out by K. Brown and others in 2009 where the emittance growth was measured for different types of foils designed at BNL, and with different β-functions at the foil location [13]. The amount of time the beam was held on the foil was varied by making the LINAC pulse width very short (50 μsec) and adjusting the timing of the injection bumps. Figure 11 (taken from [13]) shows the horizontal emittances as a function of time spent on the foil.

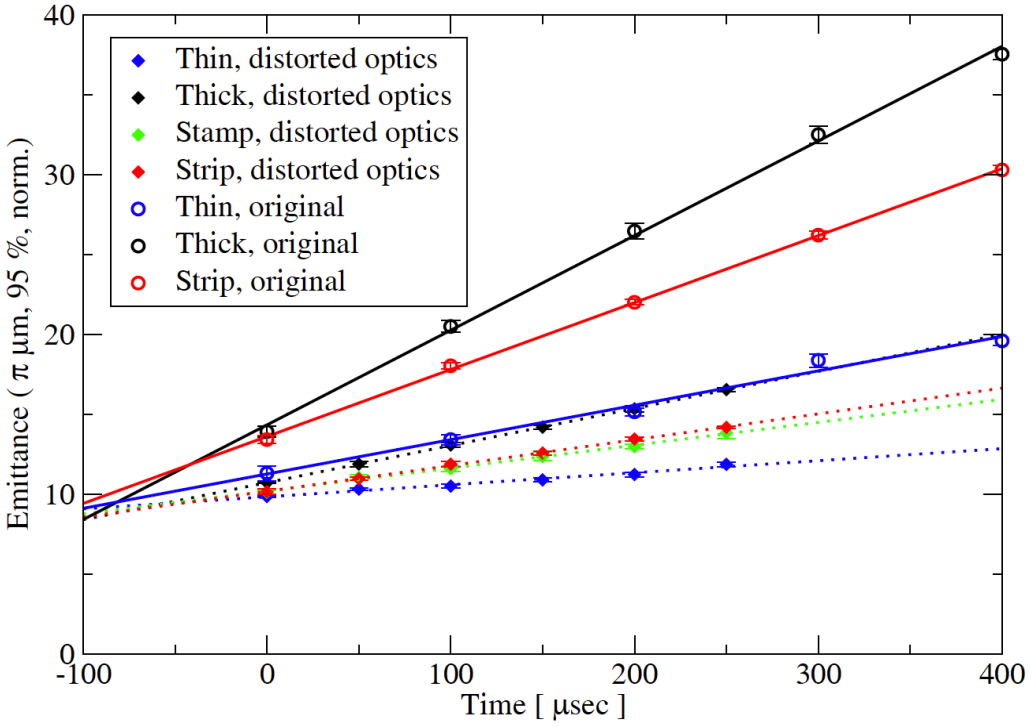

Figure 11: Emittance as a function of time spent on the foil, for different types of foils, with and without distortion of the β-function lattice.

With so much data available from direct measurements on the Booster it seems unnecessary to attempt to replicate the results through simulation. In this study, therefore, the effects of the charge exchange foil are taken into account using the measured results rather than relying on modeling.

5.3 Effects of Space Charge at Injection Energy

The goal of this part of the study is to understand how the proton beam is affected by space charge under Booster conditions at the injection energy. However, the Booster tunes change from above half-integer to away from half-integer within the 4.3 msec immediately after multi-turn injection completes. On this time scale, the beam evolves under space charge, as well as forces from the fast changing fields of the magnets. In order to identify the space charge effects under simple, stable conditions, we carry out this part of the study with the Booster fields unchanged for $\sim$4 msec.

The modeling assumes the beam is injected into the Booster ring and accumulated to the desired intensity during the first 300 μsec, just as during actual Booster operation. In the next 3.7 msec, RF capture and acceleration are not applied, and a 200 MeV coasting beam circulates in the ring, as happens in practice. However, in contrast to Booster operation, the tunes are kept at fixed values, away from integer and half-integer. Full cycle simulations with more realistic Booster conditions are reported in §6.

Simulations have been performed with five, widely ranging, intensities. The three lowest intensities cover the full range of actual proton intensities in the Booster, from very low to very high, while the other two simulations are with unrealistically high intensities in order to observe the amplified space charge effects.

Figure 12 compares the evolution of horizontal emittance (top graph) and vertical emittance (bottom graph) at the five initial intensities with set-tunes $Q_x = 4.85$, $Q_y = 4.86$ at the injection energy. Emittance growth under space charge is relatively controlled at intensities as high as 18×10^{11} but there is a marked increase in both planes at 27×10^{11}. The horizontal and vertical tune of the particles near the center of the beams are shown in Figure 13.

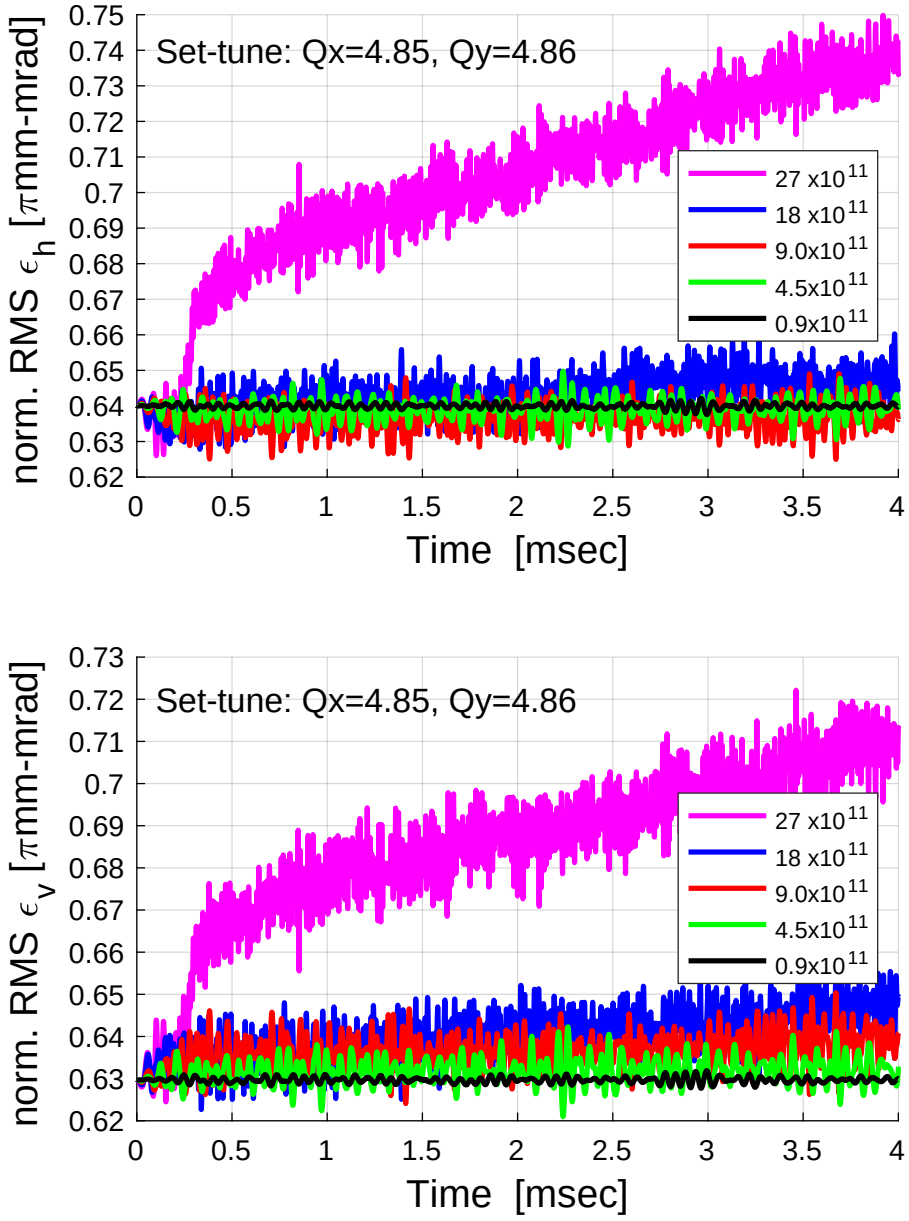

Figure 12: Evolution of horizontal emittance (top) and vertical emittance (bottom) for five different beam intensities under imaginary Booster conditions with fixed tunes of $Q_x = 4.85$, $Q_y = 4.86$.

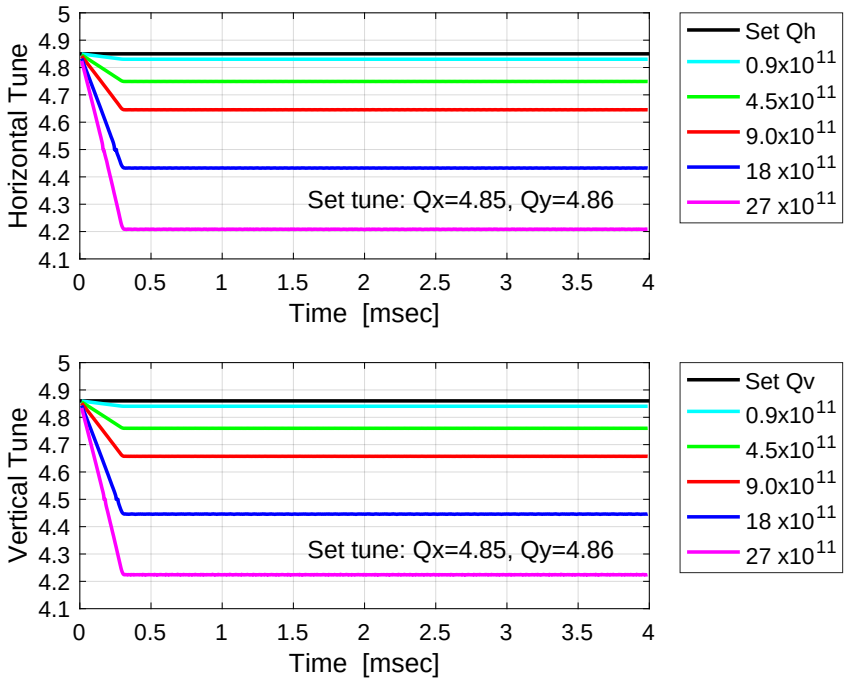

Figure 13: Horizontal (top) and vertical (bottom) tunes of the particles near the center of the beams shown in Figure 12.

Recalling remarks in §5.1, in the three cases that do correspond to real Booster levels of operation, note that these refer to the intensities of the initial circulating beam at the completion of injection, which is 10-20% less than the beam intensity that might be measured in the LINAC line.

Figure 14 compares the evolution of horizontal and vertical emittances at different initial circulating beam intensities with a different set of fixed tunes $Q_x = 4.85$ and $Q_y = 4.60$. In this case there is marked emittance growth at the lower intensity level of 18×10^{11}. The reasons for this - the values of the tunes, their relative difference, their proximity to resonances - should be addressed in the remaining sections. The corresponding horizontal and vertical tune depressions for particles close to the beam center are shown in Figure 15.

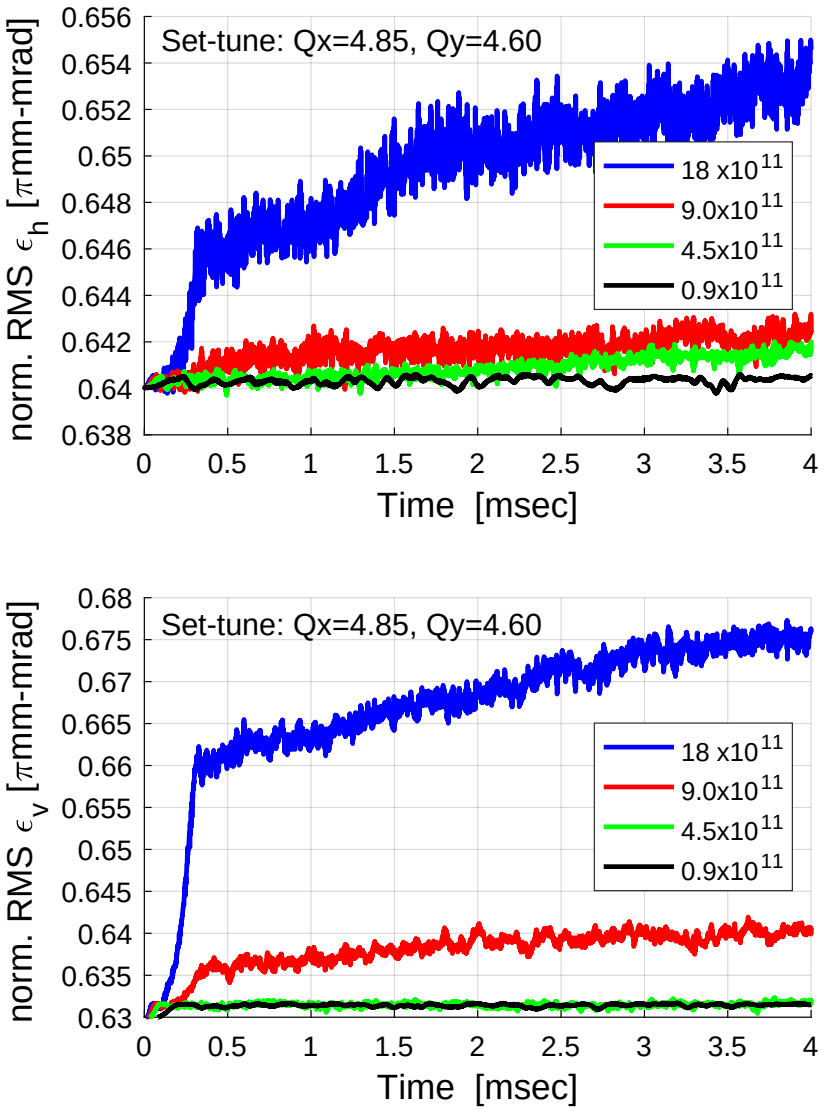

Figure 14: Evolution of horizontal emittance (top graph) and vertical emittance (bottom graph) at different initial beam intensities with fixed tunes $Q_x = 4.85, Q_y = 4.60$ at the 200 MeV injection energy.

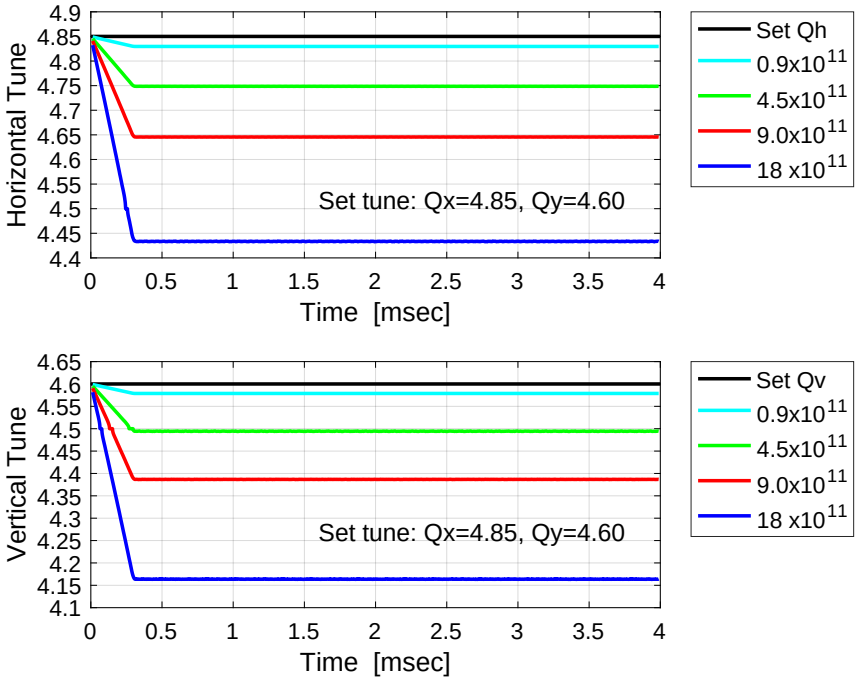

Figure 15: The horizontal tune (top graph) and vertical tune (bottom graph) of the particles near the center of the beams as shown in Figure 14.

5.4 Injection Optimization

As shown in Equation (1), the RMS emittance growth due to multiple scattering in the injection foil is proportional to the matched β-functions at the foil. It has also been demonstrated in experiments at BNL that a distorted optics could reduce the β-function at the foil, and in turn reduce the horizontal emittance [13].

The current Booster lattice at injection is designed to minimize transverse emittance growth by minimizing the β-function at the foil. Such a lattice is achieved by bringing the betatron tunes very close to the half-integer, and then distorting the lattice by exciting the half-integer stopband quadrupole strengths. However, the tune depression due to space charge could push the tunes onto the half-integer and cause emittance blowup.

There are two contradictory favorable conditions. On one hand, it is desirable to set horizontal and vertical tunes close to a half-integer in order to minimize emittance blowup in the incident beam from multiple scattering in striping foil. On the other hand, it is desirable to set horizontal and vertical tunes away from half-integers in order to minimize emittance blowup from space charge. Optimization at injection is a question of balancing the tunes between the conflicting conditions and applies both to the incident beam as the circulating beam after accumulation. An idea of which way to go is provided by our space charge simulations.

The goal of this part of study is to find the pair of best fixed tunes at which the transverse emittance blowup is minimized. This involves simulations under space charge and typical Booster conditions for a range of horizontal and vertical tunes. A scan has been carried out of 2D (Qx-Q_y) tune space covering an area just above the half-integer with Q_x ranging from 4.54 to 4.60, and Q_y ranging from 4.56 to 4.68. All other input physical and numerical parameters are kept the same, with beam intensity 9×10^{11}, $\Delta p/p = 0.64 \times 10^{-4}$ (RMS), and initial emittances (95%, normalized) $\epsilon_x = \epsilon_y = 1.5\,\pi$mm-mrad. As such simulations are CPU demanding and we need to model beam behavior for enough revolutions for space charge effects to set in, we keep the Booster lattice unchanged in this part of the study with a given pair of set-tunes.

Figure 16 summarizes the results of the tune scan, showing the evolution of horizontal and vertical (RMS) emittances during the first 4 msec following injection.

Since variances (for independent distributions) add, and emittance is a standard deviation, an indicator for the best combination of tunes is chosen to be the sum of squared emittances. On this basis, the conclusion from this part of the study is that the optimized lattice is the one with tunes of Q_x=4.60 and Q_y=4.59. At this working point, space charge tune depression brings the horizontal and vertical tunes to the point at which the RMS transverse emittance growth is minimized. This optimized working point for Booster injection is used in all full cycle simulations presented in this report.

It is interesting to point out that there is a proposal to explore some alternative lattices solutions in which the the β-functions are reduced at the foil without moving the tunes close to the half-integer. One such example has higher tunes, and the other example has tunes below the half-integer [14]. For each of these ideas, the distorted lattice optics has been produced with MADX without taking space charge effects into account. Simulations that include space charge could help to bring these ideas into reality.

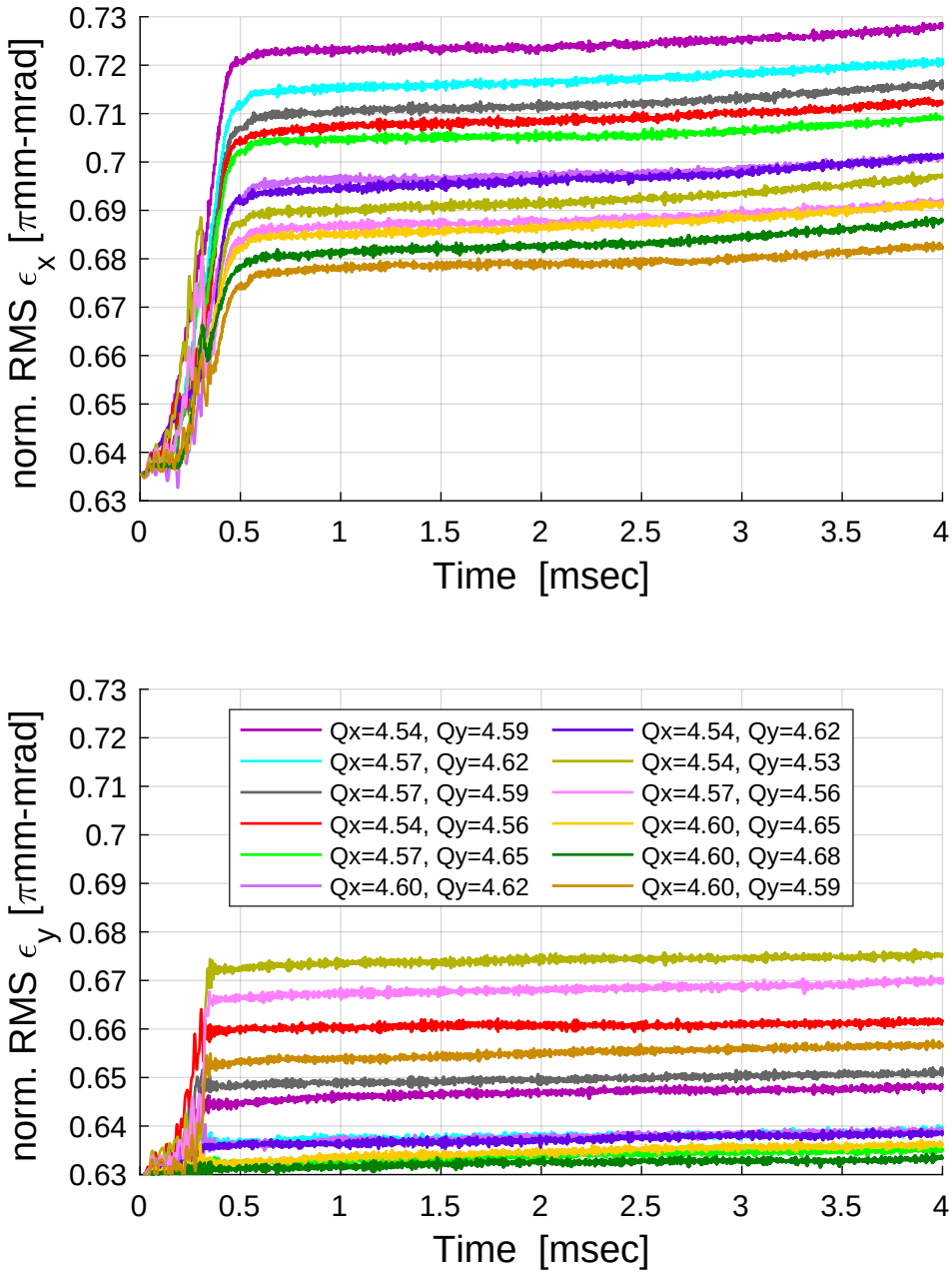

Figure 16: Evolution of horizontal emittance (top graph) and vertical emittance (bottom graph) during the first 4 msec after the completion of injection across a range of fixed tunes. Graphs are on the same scale for comparison and the color key applies to both sets of plots.

5.5 Post-injection Optimization

As described in §5.4, at injection the Booster operates with a distorted lattice that has reduced β-functions at the location of the foil, and has betatron tunes close to the half-integer in order to reduce transverse emittance growth in the stripping foil. As soon as multi-turn injection is completed, the betatron tunes need to be increased rapidly to move away from the half-integer.

At the post-injection stage, two issues need to be addressed. The first is to identify a good area in 2D tune-space where the space charge effect is not likely to cause emittance blowup due to resonance instability. The second is to find out whether the speed at which the tunes are raised plays a role and how great an impact it has on the emittance growth.

To address these two issues, in this part of study we track the beam starting from the optimized working point at injection obtained from simulations presented in the previous section to a specified post-injection working point. Each simulation tracks the beam immediately after the completion of injection in a lattice with different rates of tune increase. As with normal Booster operation, the tunes are controlled following a set of points at given times. Then the rapidity of the tune rise is characterized with the time constant obtained from curve-fit through each set of points as:

$$\begin{aligned} Q_x &= Q_{f,x} - (Q_{f,x} - Q_{i,x}) \exp(-t/\tau_x) \\ Q_y &= Q_{f,y} - (Q_{f,y} - Q_{i,y}) \exp(-t/\tau_y) \end{aligned} \tag{2}$$

where subscripts i and f refer to the initial and final values of the tunes, τ_x and τ_y are time constants, and the time t increases from $t = 0$ to a value $t \gg \max(\tau_x, \tau_y)$.

The initial set-tunes are given by the optimized working point at injection $Q_{i,x} = 4.60, Q_{i,y} = 4.59$ (as concluded in §5.4), and the final set-tunes are $Q_{f,x} = 4.81, Q_{f,y} = 4.97$, which lie in a relatively safe area in the 2D tune-plane, away from major resonance-lines, and providing some room for tune depression due to space charge.

Figure 17 shows the set-points and the corresponding curve-fits for horizontal and vertical tunes as functions of time for Booster operation (gray), and a few cases of faster tune rise with different time constants. The beam evolution during 7 mins after the tune rise are show in Figure 18. Each case presented in Figure 18 corresponds to the tune rise curve in Figure 17 of the same color.

By comparing the simulation results of these cases it can be concluded that the rate of tune increase does play a role in the beam emittance development in the later stages of the cycle. However, the impact is insignificant in the range relevant to Booster operation where the time constant is of the order of a few hundred microseconds.

The final working point in the above study is in a relatively safe area of the 2D tune-plane above the main diagonal line ($Q_{f,x} < Q_{f,y}$). The working point symmetrically located with respect to the main diagonal is also in a safe area. Accordingly we consider the case where the initial set-tunes are still the optimized values at injection ($Q_{i,x} = 4.60$, $Q_{i,y} = 4.59$), but the final set-tunes are $Q_{f,x} = 4.97$, $Q_{f,y} = 4.81$ and lie below the main diagonal in tune-space ($Q_{f,x} > Q_{f,y}$).

For this case, Figure 19 shows the set-points and their corresponding curve-fits for both horizontal and vertical tunes as functions of time with different time constants. The beam evolution during the 7 minutes after the tunes rise are shown in Figure 20, where each case corresponds to the tune rise curve in Figure 19 of the same color.

From simulation results of the cases with $Q_{f,x} > Q_{f,y}$ we conclude that the impact of the rapidity of the tune rise is insignificant in the range where the time constant is of the order of a few hundred microseconds. However, comparing Figure 20 with Figure 18 one may conclude that, when space charge effects are included, the working points below the main diagonal line ($Q_x > Q_y$)are more desirable compared to the symmetrical ones above diagonal line ($Q_x < Q_y$).

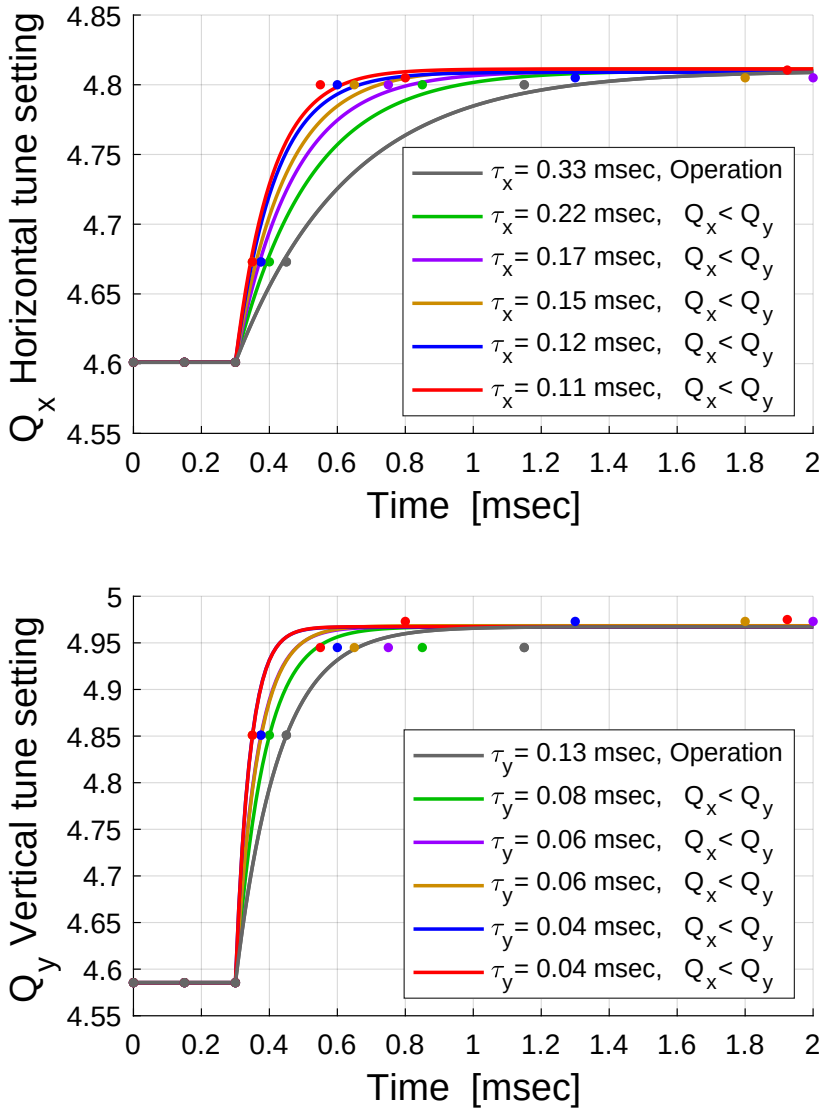

Figure 17: The set-points and their corresponding curve-fits of horizontal (top graph) and vertical (bottom graph) tunes as functions of time for Booster operation (gray), together with selected cases of faster tune rises with $Q_{f,x} < Q_{f,y}$ with different time constants.

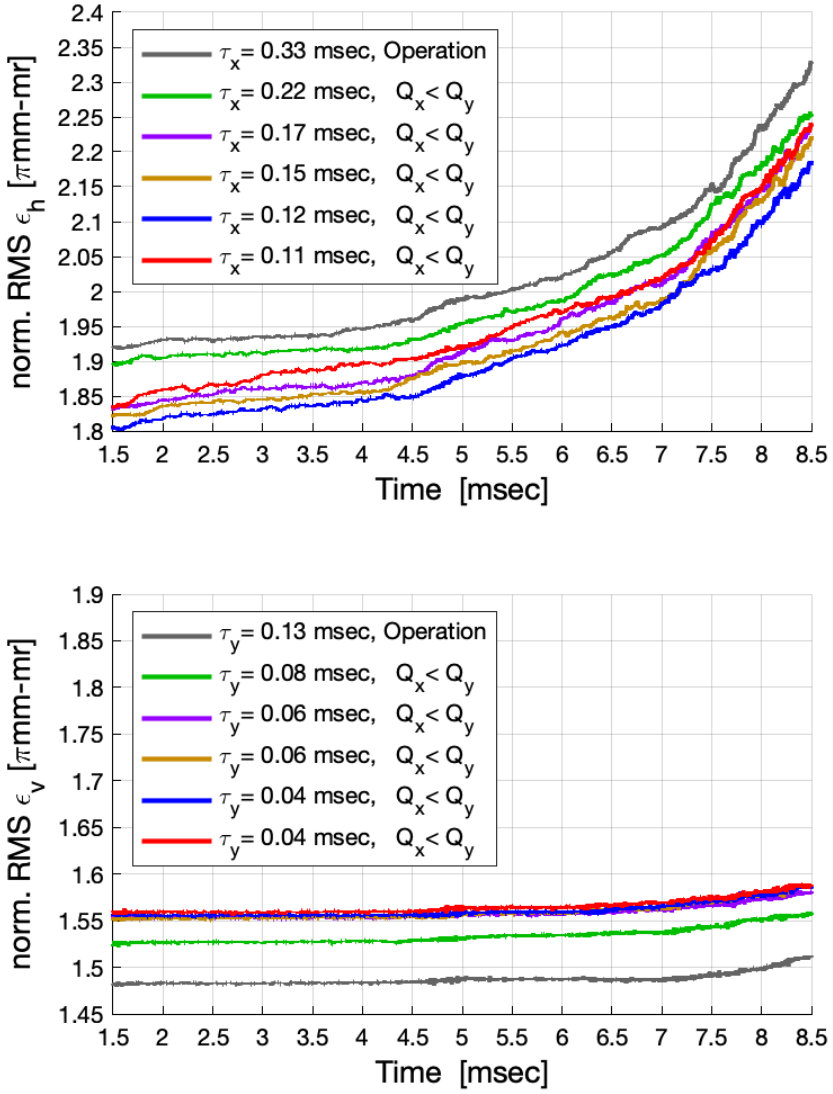

Figure 18: Evolution of horizontal and vertical emittance during the 7 msec immediately after the tunes are raised from the optimized injection working point ($Q_x = 4.60$, $Q_y = 4.59$) to a post-injection working point at $Q_x = 4.81$, $Q_y = 4.97$. The rates of tune increase correspond to the set-tunes as functions of time shown in Figure 17.

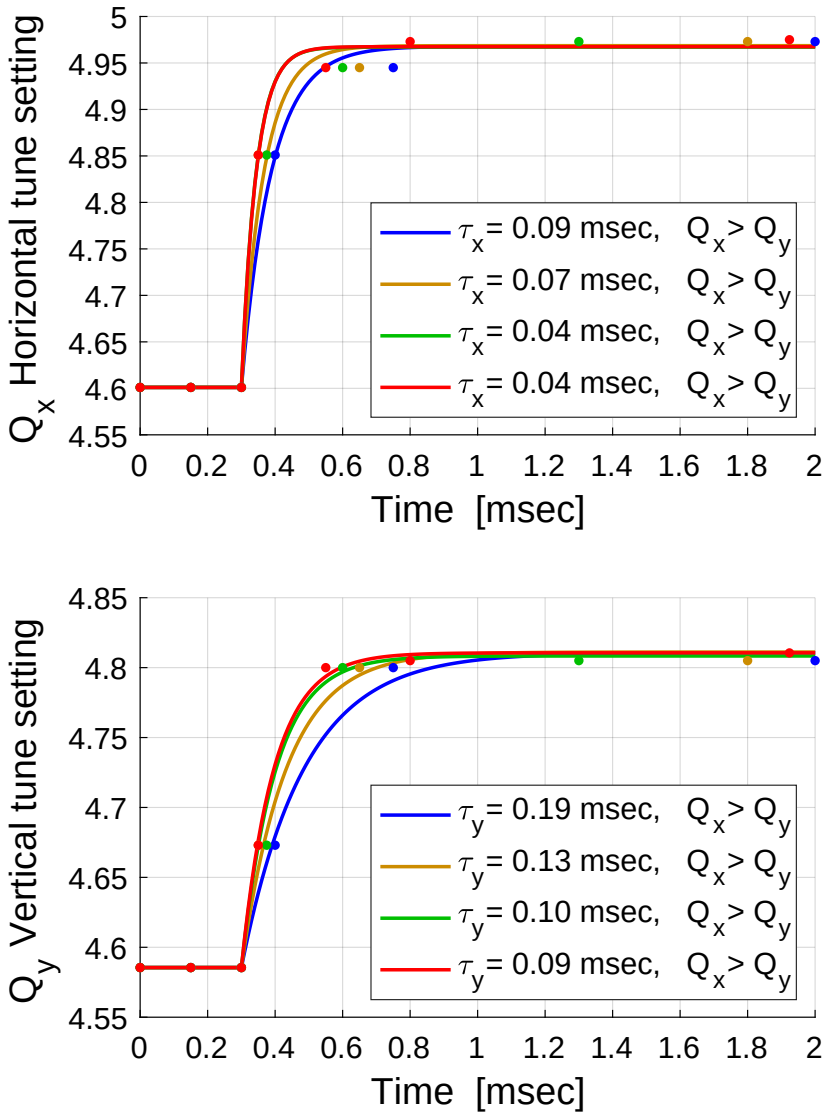

Figure 19: The set-points and their corresponding curve-fits of horizontal tunes (top graph) and vertical tunes (bottom graph) as functions of time for cases where $Q_{f,x} > Q_{f,y}$ and different time constants.

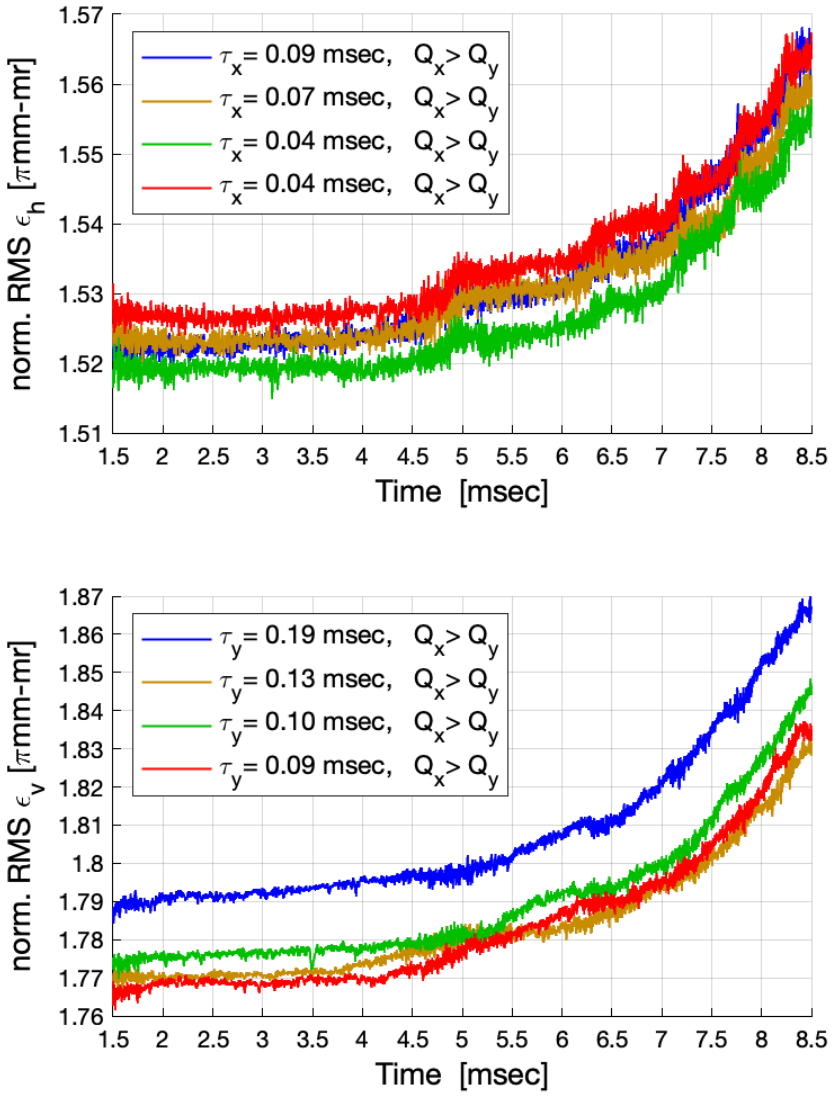

Figure 20: Evolutions of horizontal and vertical emittance during the 7 msec following tune rise from the optimized injection working point ($Q_x = 4.60$, $Q_y = 4.59$) to a post-injection working point $Q_x = 4.97$, $Q_y = 4.81$. The tunes are increased at a rate corresponding to examples shown in Figure 19.

6 Full Cycle Simulations

In each full cycle simulation of proton beams in the Booster an incident H^--beam with specified emittance and momentum spread $\Delta p/p$ is injected through a carbon foil of given thickness and tracked through the full cycle of the booster under space charge corresponding to the specified beam intensity.

In order to provide general knowledge of proton beam development through the cycle, this study is based on a large set of simulations with a wide range of beam properties including different beam intensities, different injection transverse emittances, and different injection beam momentum spread. The full cycle simulations use results from the optimizations at injection, at beam bunching, and use the tune rise timing-constant, as described in the previous sections.

In cases where parameters are not explicitly specified, the default values used in the simulations are: initial intensity=7.5×10^{11}, $\Delta p/p = 6 \times 10^{-4}$ (RMS), emittances $\epsilon_x = 3.5\,\pi$mm-mrad, $\epsilon_y = 5.5\,\pi$mm-mrad (95%, norm.) and foil thickness = $100\,\mu$g/cm^2. The hybrid model for space charge is adopted in every case.

6.1 Events and Timings in a Booster Cycle

The events of a Booster cycle for proton runs are pre-programed and automatically executed during Booster operations. Each event is triggered at a preset "Booster time" starting at BT0=0.

The multi-turn injection process starts at Booster time=71.2 msec and ends at Booster time=71.5 ms. During the 0.3 msec injection period the circulating beam intensity increases linearly from 0 to $(5 \sim 9) \times 10^{11}$ in 252 turns. The next 4.3 msec (from 71.5 to 75.8 msec) are used to remove the injection bump and move the tune away from the half-integer. RF capture starts at Booster time=75.8 msec, and ends at Booster time=77.8 msec, lasting 2 msec. This is followed by acceleration, which starts at Booster time=77.8 msec with the

RF voltage increasing according to the acceleration rate. Extraction takes place at Booster time=150 msec.

For the convenience of the simulation and graphical representation, a simulation time named "Simpsons time" is identified to be zero with an event labelled "Starts beam injection". The relationship between the operational time and the simulation time is "Booster time"= "Simpsons time"+71.2 msec. The timeline of the events during a Booster cycle is shown in Table 2. The trigger time corresponding to each event is given in both "Booster time" and "Simpsons time".

Table 2: The timeline of the events during a Booster cycle used in the full cycle simulations. Here, the relationship between the operational time and the simulation time is "Booster time"= "Simpsons time"+71.2 msec.

Booster Event	Booster Time BT0+ [msec]	Simpsons Time [msec]
Start of beam injection	71.2	0
End of beam injection	71.5	0.3
Start inj. bump removal & tune raising	71.5	0.3
"Bst-Early" beam intensity measurement	73.0	1.8
End inj. bump removal & tune raising	75.8	4.6
Start RF capture	75.8	4.6
End RF capture	77.8	6.6
Start acceleration & RF voltage increase	77.8	6.6
"Bst-Late" beam intensity measurement	120	48.8
Beam extraction	150	78.8

6.2 Energy Ramping, RF and Tunes during a Booster cycle

The operational settings of the magnetic field B and dB/dt during normal Booster energy ramping are used for these simulations. B and dB/dt are shown as functions of Simpsons time in the top graph of Figure 21.

The RF voltages of the 1st and 2nd harmonics used in the simulations are extracted from the operational setting points during a typical Booster cycle. They are shown as functions of Simpsons time in the middle graph of Figure 21. The relative phase of the 2nd harmonic in relation to the 1st RF harmonic is shown in the bottom graph of Figure 21 . The red curve is from calculation, while the blue curve is extracted from the read-back scope during a typical Booster operation, an example of which is shown in Figure 22 [15]. Here, in order to compare the two curves on the same scale, some calibration and shift have been carried out.

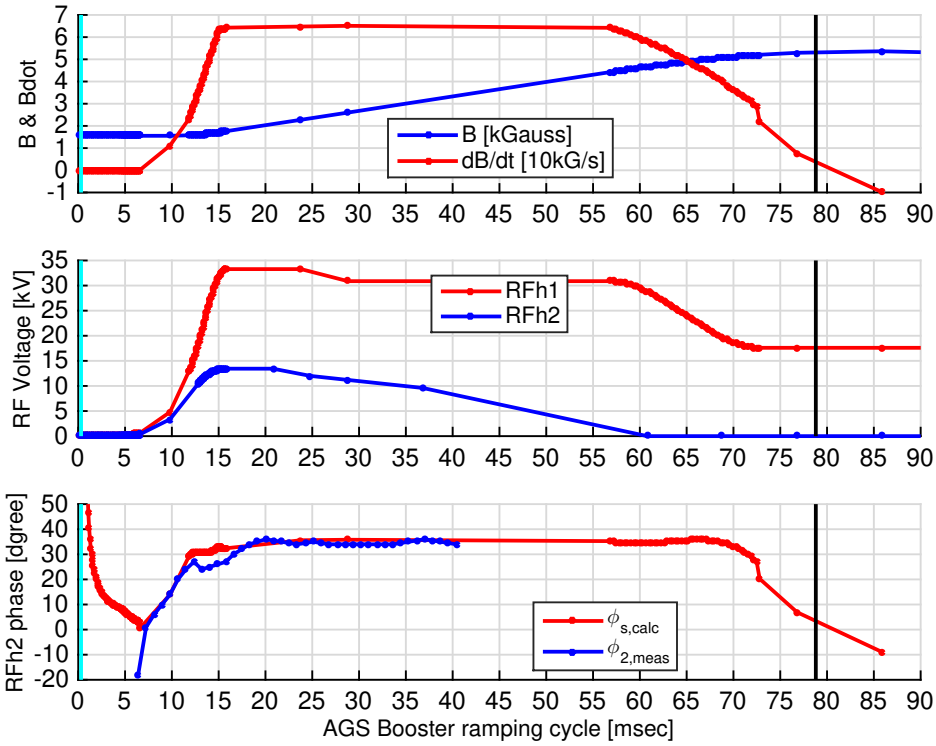

Figure 21: Some physical parameters used in the simulation of proton evolution during a Booster cycle. Top graph: magnetic field B and dB/dt; middle graph: the RF voltages of the 1st and 2nd harmonics; bottom graph: synchronous phase and relative phase of the 2nd harmonic. The red curves are from calculation; blue curves from the read-back scope during operation.

Since the run-time measurement is closer to reality, the phase of the 2nd RF harmonic from the read-back scope (blue curve in the lower graph of Figure 21) is used in the simulations. The data points beyond the values provided by the read-back scope were estimated by extrapolation.

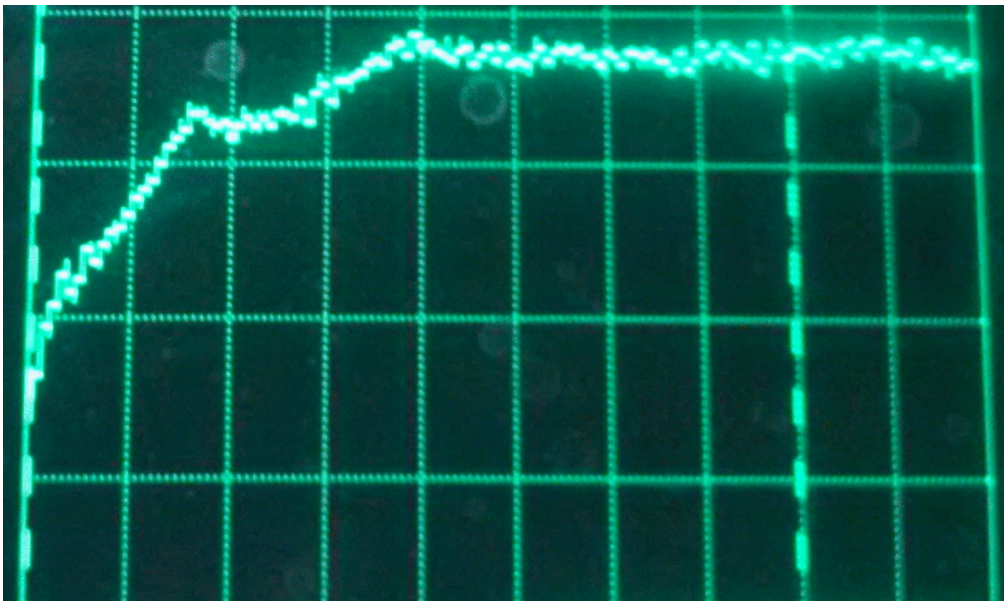

Figure 22: Relative phases of the 2nd RF harmonics in relation to the 1st RF harmonic from a read-back scope during normal Booster operation [15].

During the simulation cycle, the tunes are ramped from their initial settings of $Q_{i,x} = 4.60, Q_{i,y} = 4.59$ to final values of $Q_{f,x} = 4.81, Q_{f,y} = 4.97$ and the rapidity of the ramp is the same as in normal Booster operations. The gray dots and gray lines in Figure 17 of §5.5 show the set-points and corresponding curve-fits of the horizontal and vertical set-tunes.

6.3 Impact of Initial Intensity on a Full Cycle

Figures 23 and 24 show the evolution of transverse and longitudinal emittance, bunching factor and beam loss parameter [%] of different beam intensities under typical conditions during normal Booster operation. The BNL-designed foil has a thickness of $100\,\mu\mathrm{g/cm}^2$. The initial momentum spread $\Delta p/p = 6 \times 10^{-4}$. The total numbers of protons in the initial circulating beams used in the simulations are $N_{\mathrm{init}} = (2.5, 5, 7.5, 9) \times 10^{11}$. As described in §5.1, the beam intensities are 10-20% less than the beam intensities if measured at "Booster Input" with a current transformer in the LINAC line.

The results for transverse emittance increase are in line with expectations. However it appears that the initial intensity has almost no impact on the beams' longitudinal behaviour even with the presence of space charge. The small differences shown in Figure 24 are within the simulation error-bar, and as such are insignificant and can be neglected.

While these levels of intensity equate to the maximum achieved in Booster operation, the simulations suggest that, within the limitations of the modeling, the space charge limit has not been reached. It may also be that an increased number of macro-particles used in the modeling might disclose some more detailed effects, particularly in terms of halo formation in the transverse beam distribution.

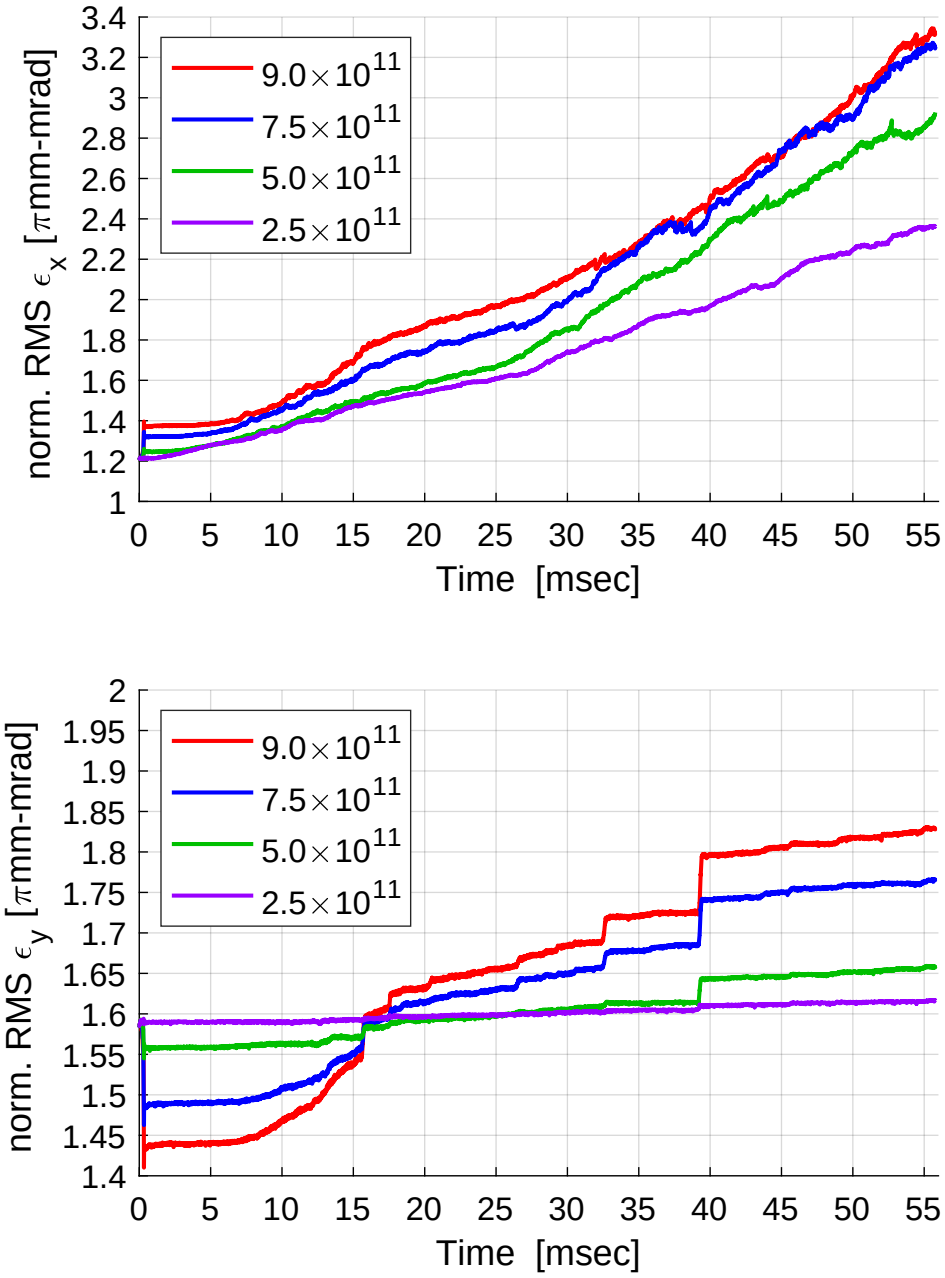

Figure 23: Evolution of horizontal emittance (top graph) and vertical emittance (bottom graph) for different initial intensities of the circulating beam under conditions corresponding to normal Booster operation.

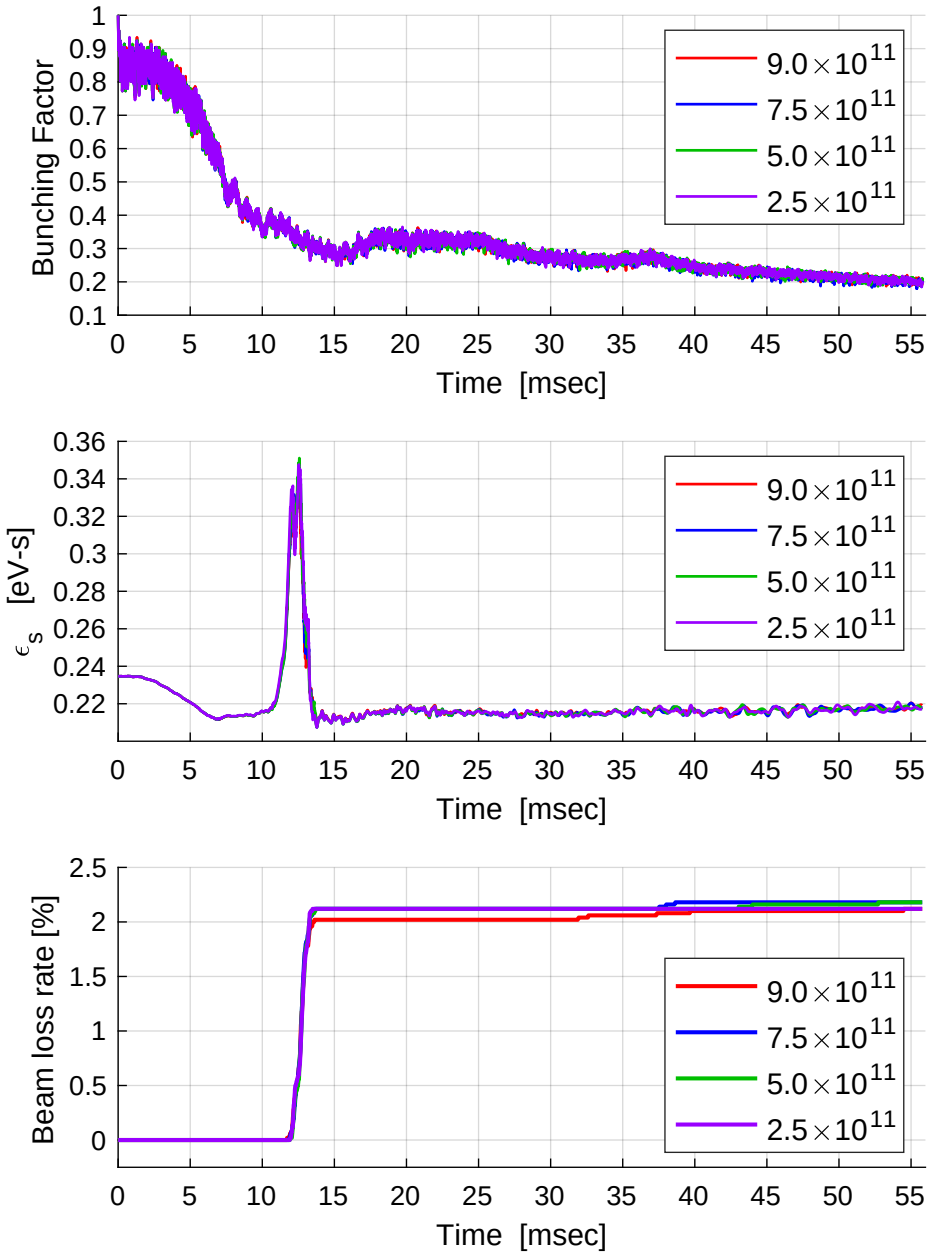

Figure 24: Evolution of longitudinal emittance (top graph), bunching factor (middle graph) and beam loss parameter [%] (bottom graph) for different initial intensities of the circulating beam under conditions of normal Booster operations.

6.4 Impact of Initial Emittance on a Full Cycle

In addition to the attempts at "realistic" simulations with the existing Booster settings, the study can also extend into the non-operational regime in order to find directions for future improvement, even if some scenarios are not practically achievable at the present time. For example, the LINAC beam might be scraped to smaller horizontal and vertical emittances before injection; or thinner carbon foils ($80\,\mu g/cm^2$ or even $50\,\mu g/cm^2$) might be used.

To answer these questions we investigate five injection schemes each with a different combination of injection conditions. as shown in Table 3.

Table 3: Injection conditions used in the full cycle simulations.

Injection Schema	#1	#2	#3	#4	#5
Horizontal emittance (95%, norm.) [πmm-mrad]	3.5	3.5	3.5	1.5	1.5
Vertical emittance (95%, norm.) [πmm-mrad]	5.5	5.5	5.5	3.5	3.5
Carbon foil thickness (BNL design) [$\mu g/cm^2$]	100	80	50	75	50

The injection schema #1 is operational in the Booster. Schemas #2 and #3 use operational emittances but with thinner carbon foils. Schemas #4 and #5 not only use thinner carbon foils, but also use much smaller emittances for the incident H^- beam. These emittances are not currently achievable.

Figures 25 and 26 show the evolution of transverse and longitudinal emittances, bunching factor and beam loss parameter [%] for the five scenarios listed in Table 3. The initial momentum spread is $\Delta p/p = 6 \times 10^{-4}$ and the total number of protons in the initial circulating beam is 7.5×10^{11}.

Comparing the evolution of horizontal emittance and vertical emittance in Figure 25, we can see similar emittance growth rates for all five cases. None of the charge densities associated with these injection schemes have reached a critical point so as to cause instability. This suggests that, if the machine is well tuned, there would be no major transverse emittance blowup in the later stages of the Booster cycle.

From this part of the study we can conclude that if we can reduce the transverse emittance of the initial circulating beam, either by scraping after LINAC, or using thinner foils, or any other method, the beam may evolve through the whole Booster cycle with the same reduced transverse emittance growth. [This, of course, ignores the fact that the lifetime of a thinner foil is likely to be less, and there will be additional partially stripped H^0 ions and unstripped H^- to be dealt with as the foil efficiency will be reduced. Also, since a large fraction of the beam loss is associated with stripping efficiency, it may be better to have a thicker foil where a larger fraction of the beam from the LINAC will circulate in the ring.]

Transverse emittance has almost no impact on a beam's longitudinal behaviour, as shown in Figure 26, in line with expectations. The small differences shown in Figure 26 fall within simulation error-bars, and can be ignored.

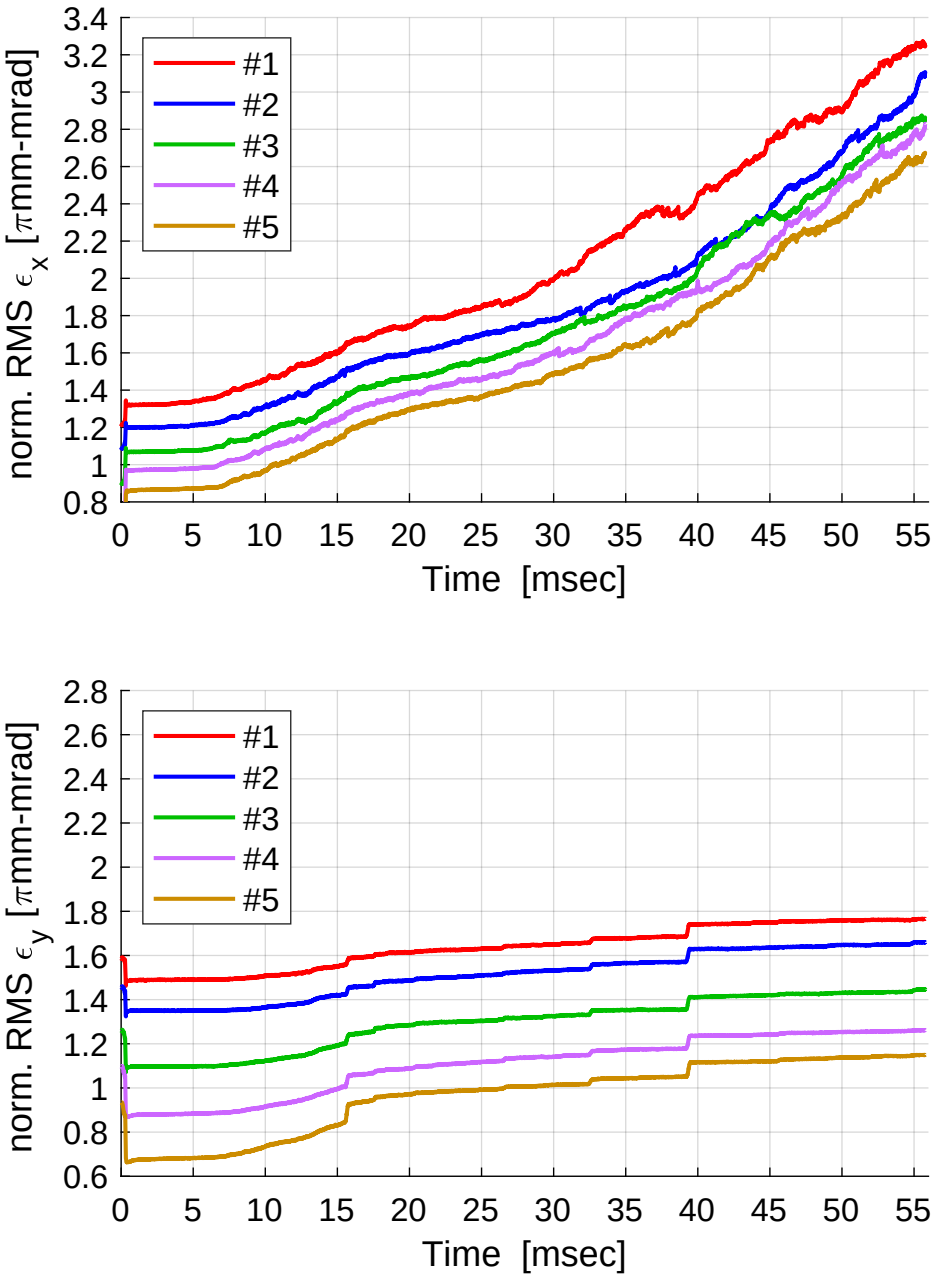

Figure 25: Evolution of horizontal emittance (top graph) and vertical emittance (bottom graph) for the five injection schema (Table 3) under the same initial conditions (initial intensity=7.5×10^{11}, initial $\Delta p/p = 6 \times 10^{-4}$ (RMS) and foil thickness = $100\,\mu\text{g/cm}^2$).

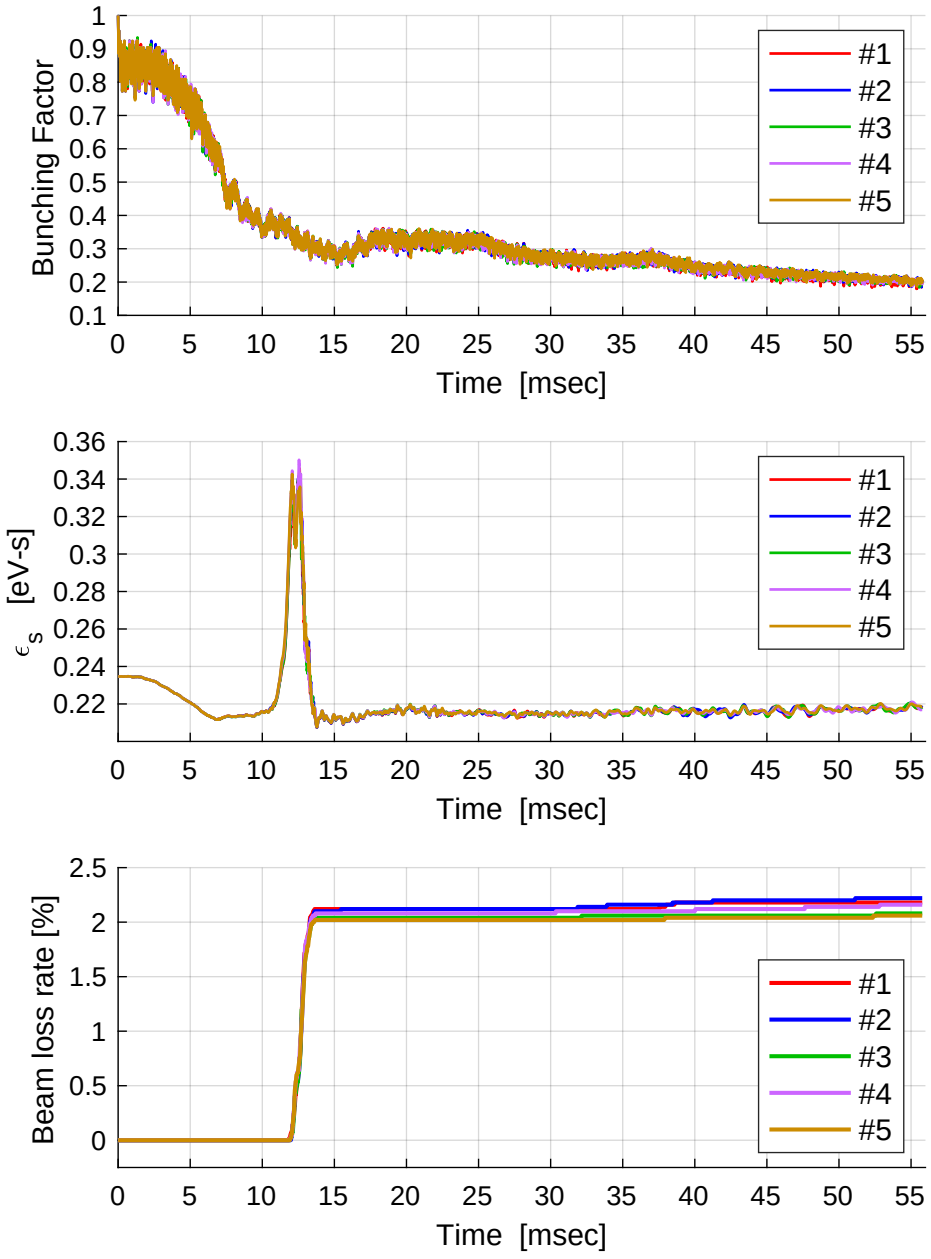

Figure 26: Details of aspects of beam evolution for the scenarios in Table 3. Top: bunching factor; middle: longitudinal emittance bottom: beam loss parameter [%]. All simulations are with the same initial conditions (intensity=7.5×10^{11}, $\Delta p/p = 6 \times 10^{-4}$ (RMS) and foil thickness = $100\,\mu\mathrm{g/cm}^2$).

6.5 Impact of Initial Momentum Spread on a Full Cycle

For each injection schema, simulations with a range of initial momentum spread have also been carried out to determine the trend of beam evolution as a function of $\Delta p/p$. Figures 27 and 28 show the evolution of transverse and longitudinal emittance, bunching factor and beam loss parameter [%] for different $\Delta p/p$ in the initial circulation beam. The loss increases with $\Delta p/p$, and is likely to be longitudinal loss since a smaller fraction of the macro-particles will fit into the stable RF region. The increase in transverse emittance appears to be lower at higher levels of $\Delta p/p$ but this will be affected by particles being lost, making comparison difficult. The sudden jumps in the vertical emittance in particular relate directly to particles hitting the machine aperture. Reducing $\Delta p/p$ to lower levels may have implications for beam stability and needs to be considered carefully.

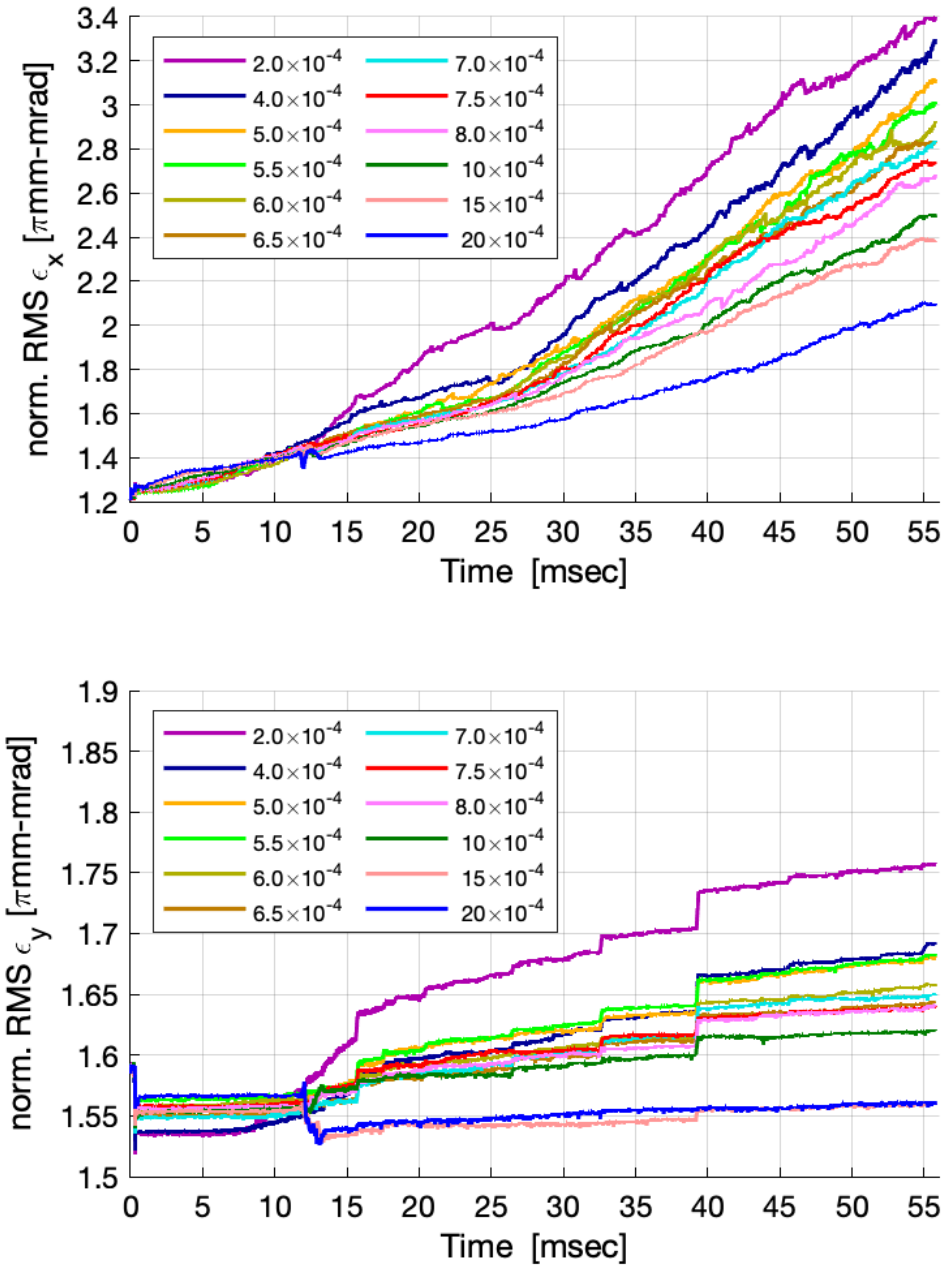

Figure 27: Evolution of horizontal emittance (top graph) and vertical emittance (bottom graph) of beams with different initial $\Delta p/p$ in the circulation beam. All these simulations are with initial intensity=5×10^{11}, initial emittances $\epsilon_x = 3.5\,\pi$mm-mrad, $\epsilon_y = 5.5\,\pi$mm-mrad (95%, norm.) and foil thickness = $100\,\mu$g/cm^2.

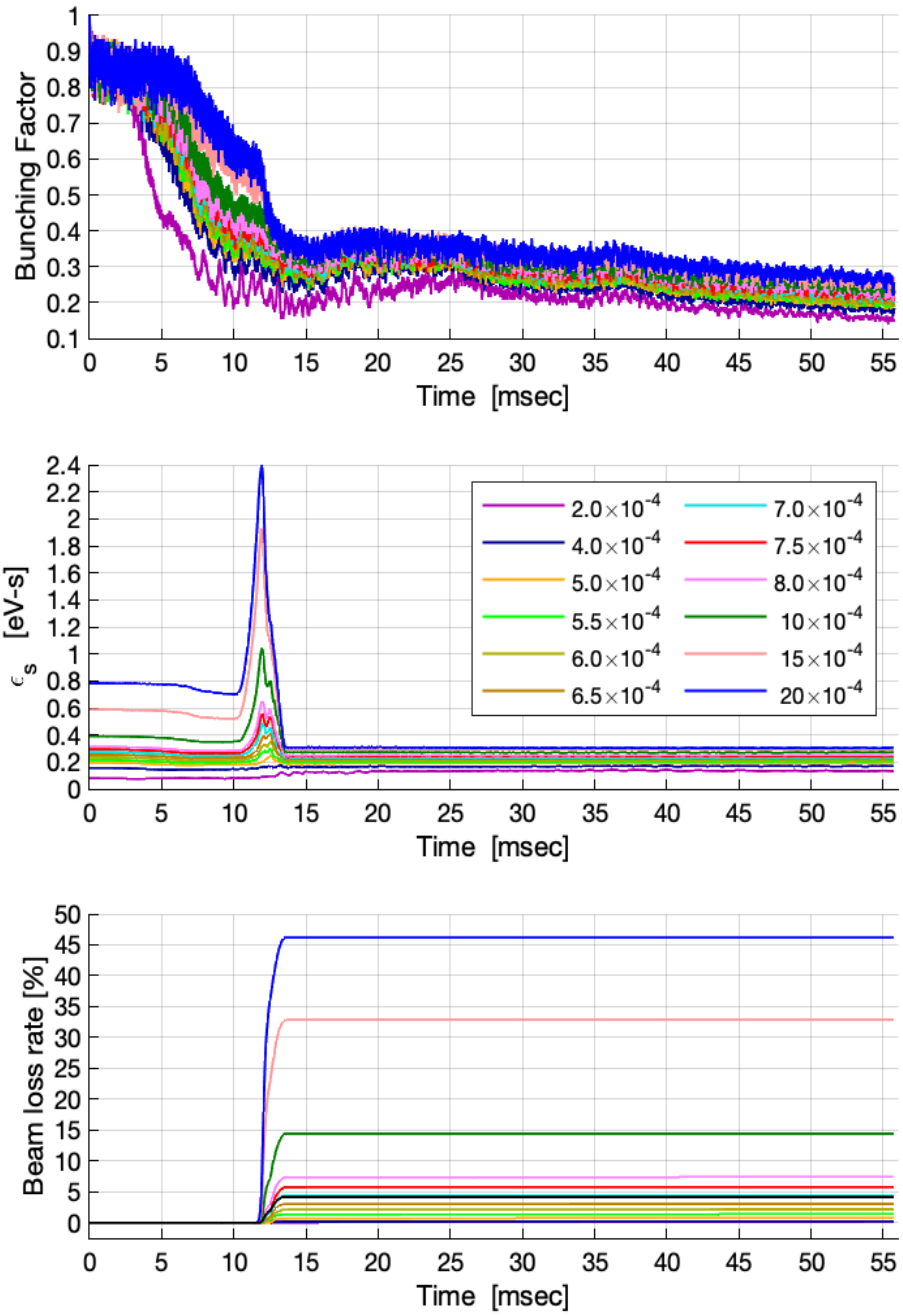

Figure 28: Evolution of bunching factor, longitudinal emittance and beam loss parameter [%] for different initial $\Delta p/p$ in the circulation beam. All these simulations are with initial intensity=5×10^{11}, initial emittances $\epsilon_x = 3.5\,\pi$mm-mrad, $\epsilon_y = 5.5\,\pi$mm-mrad (95%, norm.) and foil thickness $= 100\,\mu$g/cm^2.

6.6 Trends in Beam Properties and Parameter Changes

It would be helpful to explore trends in beam properties during evolution through a full Booster cycle in the hope that quantitative relationships can be established between the injected and extracted beams. By examining the figures presented in the previous three subsections (§6.3, §6.4 and §6.5) it can be seen that the beam parameters tend towards a steady state in the latter stages of the Booster cycle. The average value over the last 1 msec of any of the graphs in Figures 23 through 28 can be taken to represent the final value of that beam property parameter at beam extraction.

Every such final value is the result of beam evolution through a Booster cycle starting with a specific set of beam property parameters, such as intensity, emittance or $\Delta p/p$. There is a one-on-one relationship between injected and extracted beams for any given set of machine conditions.

To investigate the trend of changes in any beam property from injection to extraction, we have performed a sequence of simulations where the only difference is the initial value of the one beam parameter under investigation. All other initial properties and machine conditions are kept same for each simulation in the group. The trend of the beam property change can be realized when the final value (calculated by averaging over the last 1 msec) versus the initial value are plotted in the same graph.

Figures 29 and 30 show the trend in horizontal and vertical emittance, respectively. In these two figures, simulations are first grouped by four different beam intensities. They are plotted into four sub-figures labeled by the value of the initial intensity, $N_{\text{init}} = 2.5 \times 10^{11}$, 5×10^{11}, 7.5×10^{11} and 9×10^{11}. The simulations are further grouped into five sub-groups represented by different colors within each group. Each simulation within a sub-group has the same initial transverse emittance corresponding to one of the injection schema listed in Table 3. A transverse emittance at extraction (averaged over the last 1 msec) obtained from one simulation is plotted as one point against its initial $\Delta p/p$. Different colored curves are obtained from the data points by applying a 2^{nd} order polynomial fit.

Trends in longitudinal emittance, bunching factor and accumulated beam

loss at extraction are shown in Figure 31. Groups of simulations are color-coded according to the four different values of N_{init}, and, as above, data points provide the input for second-order polynomial fits.

With the aid of these trend graphs in Figures 29 to 31 one will be able to predict likely extracted beam properties from the injected beam parameters.

We take a case as an example. Assuming a beam is injected into the Booster with momentum spread $\Delta p/p = 6 \times 10^{-4}$ and initial intensity 5×10^{11} (which in reality should corresponds to $(5.6 \sim 6.3) \times 10^{11}$ if measured in the LINAC line at *Bst_Input*) and the injection schema is #1 ($\epsilon_h = 3.5\,\pi$mm-mrad, $\epsilon_v = 5.5\,\pi$mm-mrad, carbon foil thickness $100\,\mu\text{g/cm}^2$), we get the estimated horizontal and vertical emittance of the extracted beam to be $2.9\,\pi$mm-mrad and $1.7\,\pi$mm-mrad respectively (red curves in upper right plots of Figures 29 and 30). Similarly, from Figure 31 we get the the estimated longitudinal emittance, bunching factor and accumulated beam loss of the extracted beam to be 22 meV-s, 0.2 and 3% (excluding loss at the foil).

Note that these simulations do not include magnet errors, noise and mismatch that may exist in the real machine. They do, however, include unavoidable numerical rounding and other errors and noise because of the limited number of macro-particles. With these provisos, these trend graphs can be used to quantify the evolution of well-behaved beams in a well-tuned Booster, effectively identifying a "best case scenario".

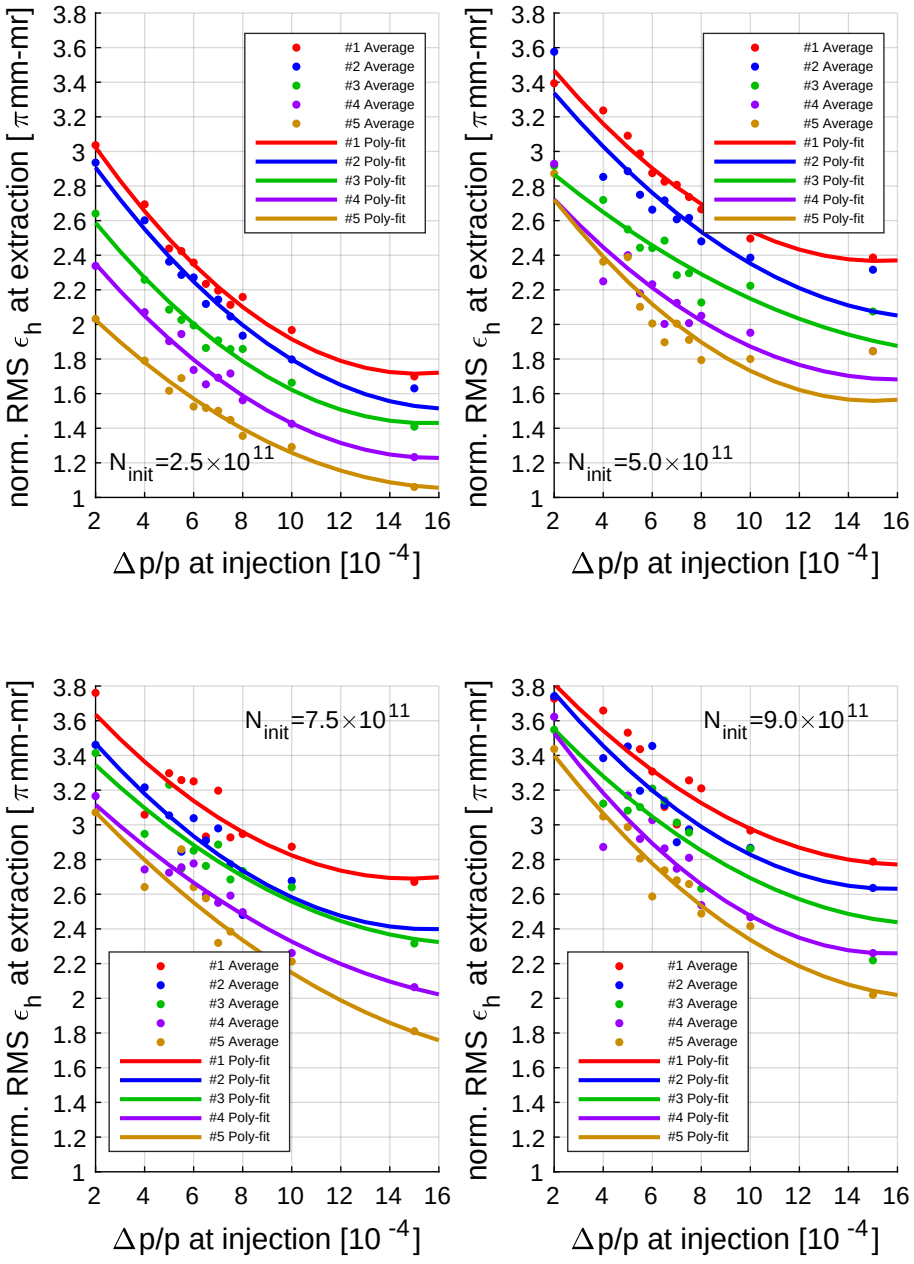

Figure 29: Trend in horizontal emittance for varying initial $\Delta p/p$ with initial intensities of $N_{\text{init}} = (2.5, 5, 7.5, 9) \times 10^{11}$ shown in sub-figure 1, 2, 3, 4, respectively.

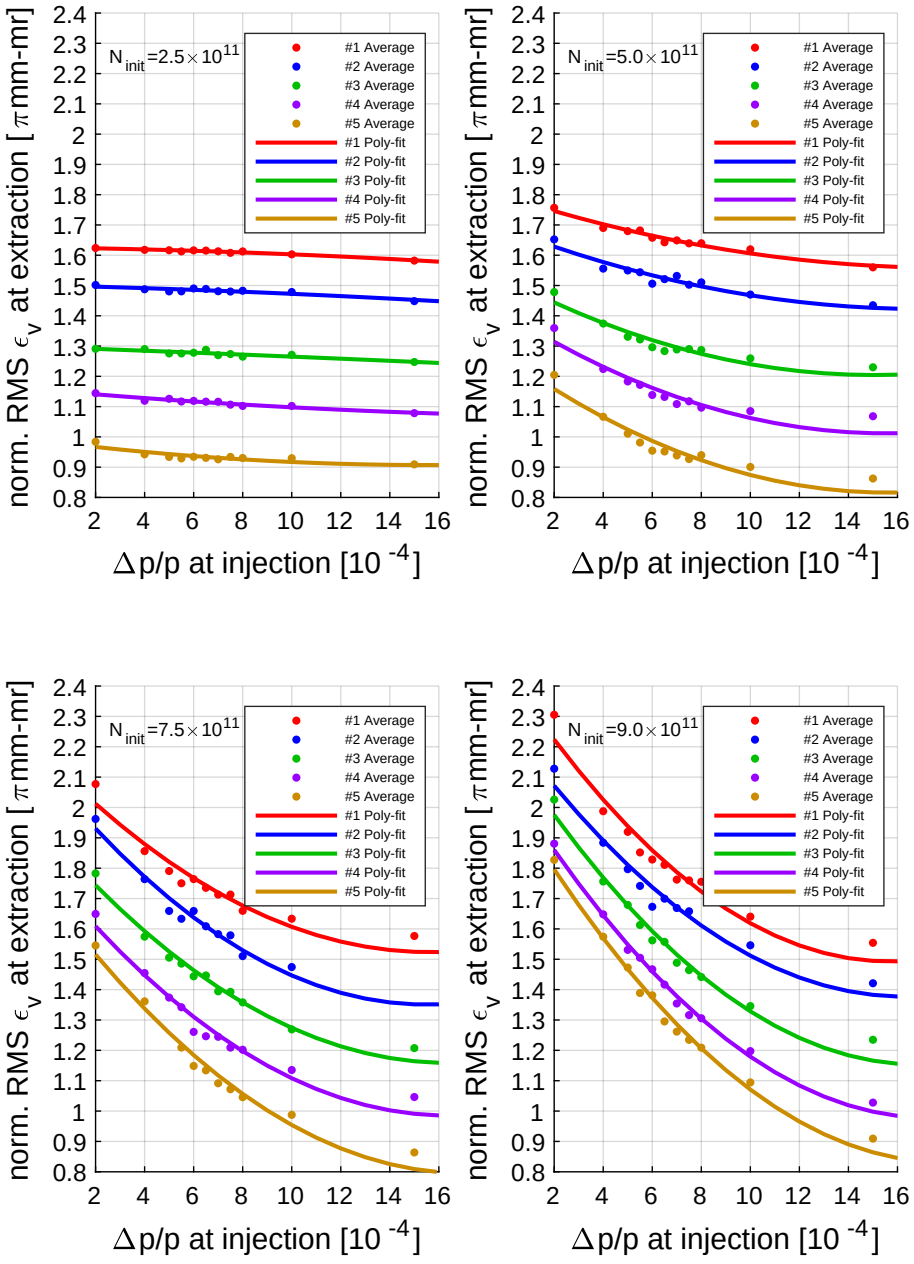

Figure 30: Trend in vertical emittance for varying initial $\Delta p/p$ with initial intensities of $N_{\text{init}} = (2.5, 5, 7.5, 9) \times 10^{11}$ shown in sub-figure 1, 2, 3, 4, respectively.

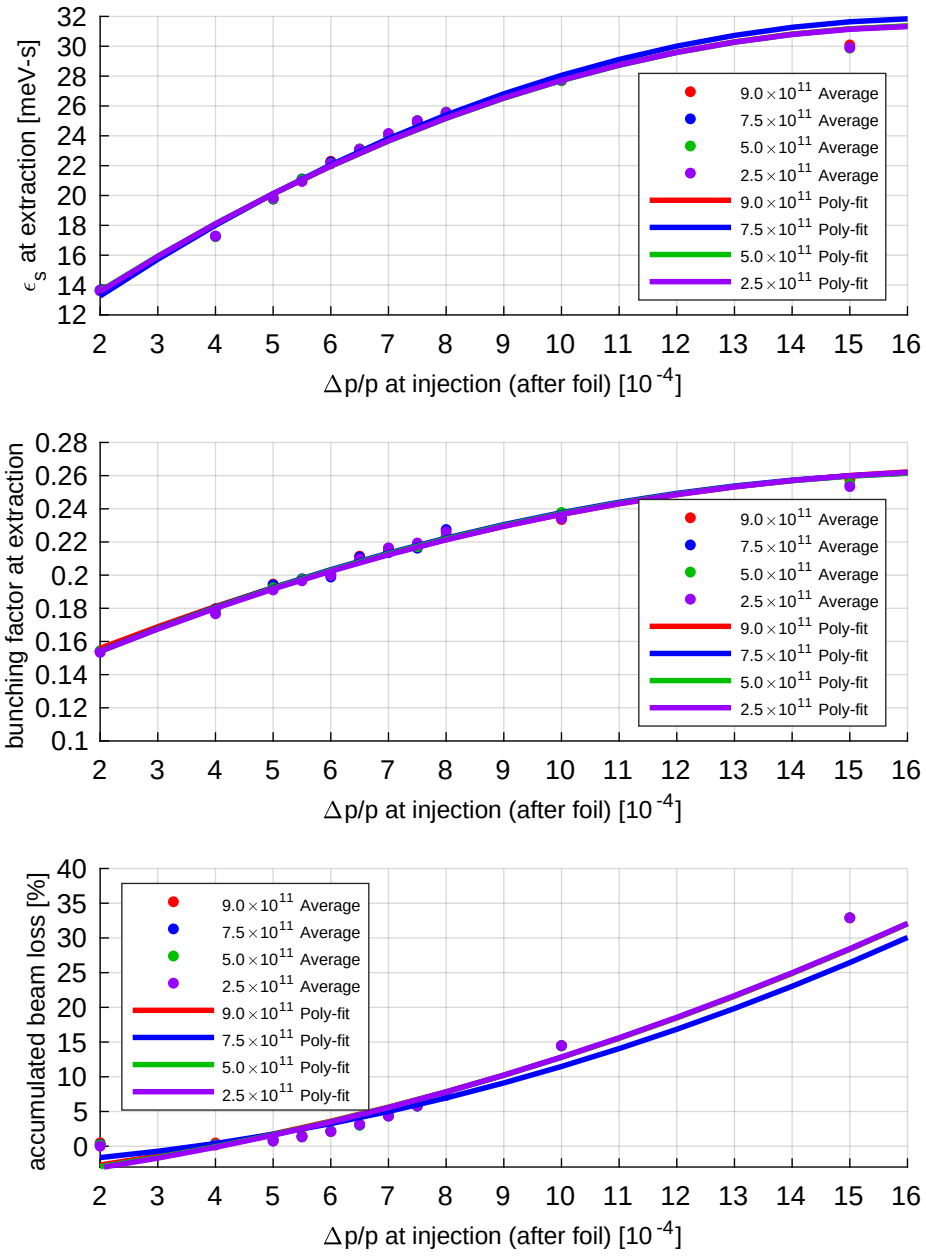

Figure 31: Trends in longitudinal emittance, bunching factor and accumulated beam loss at extraction as functions of initial $\Delta p/p$.

7 Summary and discussion

Investigations into beam dynamics in the AGS Booster have been performed using computer simulations including space charge, allied to known parameters and features of the machine.

A hybrid model for simulating space charge in circulating beams has been introduced and applied at BNL for the first time. It is aimed at long-term tracking when major changes in beam evolution can be relatively slow and calculates space charge from a "frozen" model of the beam distribution that is updated only when circumstances dictate.

In this report, this model and its implementation into the established "Simpsons" computer code are described. Confidence in the hybrid model in particular and Simpsons in general is based on thorough benchmarking in dedicated programs over a number of years, code-on-code and code against run-time measurements on real machines (at CERN, GSI, J-PARC and ORNL). Good agreement has been obtained. In view of the requirements, the code was readily deemed suitable for the beam dynamics study on the Booster at BNL.

The investigation is split into two major parts. The first covers beam injection and the early stages of the Booster cycle where significant portions of the total beam loss are found and major contributions to emittance growth take place. The focus of the study in this part was to investigate when and where the beam is lost, when and where the emittance blows up and find possible mitigation through optimization. The second part concerns modeling of the full Booster cycle with realistic operational settings or run-time read-backs during normal Booster operation. The aim here was to find the trends in changing beam properties through a full cycle by establishing quantitative relationships between parameters in the injected and extracted beams.

In this study, beam loss during the earlier part of the Booster cycle was assessed using four sets of beam intensity data collected during different runs. The rates turn out to be remarkably consistent ranging from 15% to 20% with an average of 17%. Closer examination confirms that a large fraction of the beam loss is associated with the stripping efficiency of the charge exchange

injection foil. For the incident H^- beam at 200 MeV on the BNL-designed carbon foil with thickness 100 $\mu g/cm^2$, the estimated loss is 9%. In addition, there is possible beam loss of 0-10% in the LTB-line, and a further possible beam loss of a few % due to injection mismatch. Together, these account 10-20% particle loss before the proton beam even starts circulating in the ring.

The beam loss in the later part of Booster cycle happens at 11.8 msec timed from the injection trigger. A closer investigation indicates that the beam loss is mainly longitudinal and due to particles that have fallen outside the RF bucket.

Optimizations have been performed at various stages of the Booster cycle covering features such as injection, beam bunching, and tune ramping, using simulations that take into account space charge effects. Full cycle simulations with space charge were carried out using the optimized tunes and timings for a range of beam properties, including intensity, emittance, and momentum spread.

The approach of finding the trends of beam property changes during evolution by establishing quantitative relationships between parameters at different times, proposed in §6.6 has potential beyond this simulation study. An AI (artificial intelligence) system could conceivably be developed at real time and used to guide accelerator operations.

These studies have essentially been based on the Booster as it presently operates and trying to identify sources of beam loss and emittance growth. Further studies might consider finding theoretical alternative procedures to try to reduce the loss, whether through direct operating procedures or through mechanisms designed to improve parameter stability against progressive effects (mostly space charge effect). A revised RF voltage ramp and the 2^{nd} to 1^{st} harmonic phase variation could reduce the longitudinal beam loss resulting from particles finding their way out of the RF bucket. A revised orbit bump program at injection could reduce the number of protons traversing the injection foil, thereby reducing foil heating and improving foil lifetime. A revised foil thickness might improve stripping efficiency and reduce the effects of scattering. Some ideas are amenable to experiment in the Booster ring; others can only be studied using simulation. The simulation runs may need

to be repeated with a greatly increased number of macro-particles ($> 10^6$). The modeling here has looked mainly at RMS effects and the number of particles used is inadequate to study halo formation, non-linear space-charge effects and the onset of instabilities in detail.

With this enhanced program, the ideas put forward in §6.6 could provide an AI system that could be built into a system controlling machine operation through machine learning based on a rich and varied knowledge of Booster characteristics and parameter behavior.

References

[1] I. Hofmann, "Space Charge Physics for Particle Accelerators", Springer (2017)

[2] J. Struckmeier, "Stochastic effects in real and simulated charged particle beams", Phys. Rev. ST, Accel. and Beams 3, 034202 (2000)

[3] J. Beebe-Wang, A.U. Luccio, N. D'Imperio, S. Machida, "Space Charge Simulation Methods Incorporated in Some Multi-particle Tracking Codes and Their Results Comparison", Proceedings of EPAC2002, p1329-1331, Paris, France (2002)

[4] I. Hofmann, et al, "Stability of the Kapchinskij-Vladimirskij (K-V) Distribution in Long Periodic Transport Systems", Part. Accel. 13 (1983) 145

[5] S. Machida, "Benchmarking and Application of Space Charge Codes for Rings", Proceedings of IPAC15, p2402-2407, Richmond, VA, USA (2015)

[6] A. Oeftiger, "Symplecticity in Space Charge Codes", presented at Space-Charge 2015, Oxford, UK, unpublished (2015)

[7] H. Hotchi, "Beam Commissioning and Operation of the Japan Proton Accelerator Research Complex 3-GeV Rapid Cycling Synchrotron", Prog. Theor. Exp. Phys. 2012, 02B003 (2012)

[8] K. Ohmi, et al, "Simulation of Space Charge Effects in JPARC", Proceedings of IPAC10, p. 4677-4679, Kyoto, Japan (2010)

[9] Booster-AGS-pp Elog, Entry 2022 Apr 14 13:46, BNL (2022)

[10] K. Zeno, BNL, private communication

[11] D. Raparia, BNL, private communication

[12] C.J. Gardner, "Emittance growth due to multiple passes through H-minus stripping foil in Booster", BNL Tech-Note, BNL-113654-2017-TECH (2017)

[13] K.A. Brown, L. Ahrens, C. Gardner, D. Gassner, D. Raparia, D. Steski, P. Thieberger, K. Zeno, "Minimizing Emittance Growth During H^- Injection in the AGS Booster", Proceedings of PAC09, p3729-3731, Vancouver, BC, Canada (2009)

[14] C. Liu, J. Beebe-Wang, K. Brown, C. Gardner, H. Huang, M. Minty, V. Schoefer, K. Zeno, "Rematching AGS Booster Synchrotron Injection Lattice for Smaller Transverse Beam Emittances", Proceedings of IPAC2017, p.3353-3355, Copenhagen, Denmark, (2017)

[15] F. Severino, BNL, private communication